Dark Energy Survey year 1 results: Constraints on extended cosmological models from galaxy clustering and weak lensing

T. M. C. Abbott *et al.* (DES Collaboration)

Dark Energy Survey Year 1 Results:
Constraints on Extended Cosmological Models from Galaxy Clustering and Weak Lensing

T. M. C. Abbott,[1] F. B. Abdalla,[2,3] S. Avila,[4] M. Banerji,[5,6] E. Baxter,[7] K. Bechtol,[8] M. R. Becker,[9] E. Bertin,[10,11]
J. Blazek,[12,13] S. L. Bridle,[14] D. Brooks,[2] D. Brout,[7] D. L. Burke,[15,16] A. Campos,[17,18] A. Carnero Rosell,[19,20]
M. Carrasco Kind,[21,22] J. Carretero,[23] F. J. Castander,[24,25] R. Cawthon,[26] C. Chang,[26] A. Chen,[27] M. Crocce,[24,25]
C. E. Cunha,[15] L. N. da Costa,[20,19] C. Davis,[15] J. De Vicente,[28] J. DeRose,[29,15] S. Desai,[30] E. Di Valentino,[14] H. T. Diehl,[31]
J. P. Dietrich,[32,33] S. Dodelson,[18] P. Doel,[2] A. Drlica-Wagner,[31] T. F. Eifler,[34,35] J. Elvin-Poole,[14,12] A. E. Evrard,[36,27]
E. Fernandez,[23] A. Ferté,[37,38,39] B. Flaugher,[31] P. Fosalba,[25,24] J. Frieman,[31,26] J. García-Bellido,[40] E. Gaztanaga,[25,24]
D. W. Gerdes,[27,36] T. Giannantonio,[6,5,41] D. Gruen,[15,16] R. A. Gruendl,[21,22] J. Gschwend,[20,19] G. Gutierrez,[31] W. G. Hartley,[2,42]
D. L. Hollowood,[43] K. Honscheid,[12,44] B. Hoyle,[45,41] D. Huterer,[27] B. Jain,[7] T. Jeltema,[43] M. W. G. Johnson,[22]
M. D. Johnson,[22] A. G. Kim,[46] E. Krause,[35] K. Kuehn,[47] N. Kuropatkin,[31] O. Lahav,[2] S. Lee,[44,12] P. Lemos,[5,6] C. D. Leonard,[18]
T. S. Li,[26,31] A. R. Liddle,[37] M. Lima,[19,48] H. Lin,[31] M. A. G. Maia,[19,20] J. L. Marshall,[49] P. Martini,[50,12] F. Menanteau,[22,21]
C. J. Miller,[27,36] R. Miquel,[23,51] V. Miranda,[35] J. J. Mohr,[45,33,32] J. Muir,[15] R. C. Nichol,[4] B. Nord,[31] R. L. C. Ogando,[20,19]
A. A. Plazas,[34] M. Raveri,[26] R. P. Rollins,[14] A. K. Romer,[52] A. Roodman,[15,16] R. Rosenfeld,[19,53] S. Samuroff,[18] E. Sanchez,[28]
V. Scarpine,[31] R. Schindler,[16] M. Schubnell,[27] D. Scolnic,[26] L. F. Secco,[7] S. Serrano,[25,24] I. Sevilla-Noarbe,[28] M. Smith,[54]
M. Soares-Santos,[55] F. Sobreira,[19,56] E. Suchyta,[57] M. E. C. Swanson,[22] G. Tarle,[27] D. Thomas,[4] M. A. Troxel,[12,44]
V. Vikram,[9] A. R. Walker,[1] N. Weaverdyck,[27] R. H. Wechsler,[16,29,15] J. Weller,[32,45,41] B. Yanny,[31] Y. Zhang,[31] and J. Zuntz[37]

(DES Collaboration)

[1]*Cerro Tololo Inter-American Observatory, National Optical Astronomy Observatory, Casilla 603, La Serena, Chile*
[2]*Department of Physics & Astronomy, University College London, Gower Street, London, WC1E 6BT, UK*
[3]*Department of Physics and Electronics, Rhodes University, PO Box 94, Grahamstown, 6140, South Africa*
[4]*Institute of Cosmology & Gravitation, University of Portsmouth, Portsmouth, PO1 3FX, UK*
[5]*Kavli Institute for Cosmology, University of Cambridge, Madingley Road, Cambridge CB3 0HA, UK*
[6]*Institute of Astronomy, University of Cambridge, Madingley Road, Cambridge CB3 0HA, UK*
[7]*Department of Physics and Astronomy, University of Pennsylvania, Philadelphia, PA 19104, USA*
[8]*LSST, 933 North Cherry Avenue, Tucson, AZ 85721, USA*
[9]*Argonne National Laboratory, 9700 South Cass Avenue, Lemont, IL 60439, USA*
[10]*CNRS, UMR 7095, Institut d'Astrophysique de Paris, F-75014, Paris, France*
[11]*Sorbonne Universités, UPMC Univ Paris 06, UMR 7095,*
Institut d'Astrophysique de Paris, F-75014, Paris, France
[12]*Center for Cosmology and Astro-Particle Physics, The Ohio State University, Columbus, OH 43210, USA*
[13]*Institute of Physics, Laboratory of Astrophysics, École Polytechnique Fédérale*
de Lausanne (EPFL), Observatoire de Sauverny, 1290 Versoix, Switzerland
[14]*Jodrell Bank Center for Astrophysics, School of Physics and Astronomy,*
University of Manchester, Oxford Road, Manchester, M13 9PL, UK
[15]*Kavli Institute for Particle Astrophysics & Cosmology,*
P. O. Box 2450, Stanford University, Stanford, CA 94305, USA
[16]*SLAC National Accelerator Laboratory, Menlo Park, CA 94025, USA*
[17]*Instituto de Física Teórica, Universidade Estadual Paulista, São Paulo, Brazil*
[18]*Department of Physics, Carnegie Mellon University, Pittsburgh, Pennsylvania 15213, USA*
[19]*Laboratório Interinstitucional de e-Astronomia - LIneA,*
Rua Gal. José Cristino 77, Rio de Janeiro, RJ - 20921-400, Brazil
[20]*Observatório Nacional, Rua Gal. José Cristino 77, Rio de Janeiro, RJ - 20921-400, Brazil*
[21]*Department of Astronomy, University of Illinois at Urbana-Champaign, 1002 W. Green Street, Urbana, IL 61801, USA*
[22]*National Center for Supercomputing Applications, 1205 West Clark St., Urbana, IL 61801, USA*
[23]*Institut de Física d'Altes Energies (IFAE), The Barcelona Institute of*
Science and Technology, Campus UAB, 08193 Bellaterra (Barcelona) Spain
[24]*Institute of Space Sciences (ICE, CSIC), Campus UAB,*
Carrer de Can Magrans, s/n, 08193 Barcelona, Spain
[25]*Institut d'Estudis Espacials de Catalunya (IEEC), 08193 Barcelona, Spain*
[26]*Kavli Institute for Cosmological Physics, University of Chicago, Chicago, IL 60637, USA*
[27]*Department of Physics, University of Michigan, Ann Arbor, MI 48109, USA*
[28]*Centro de Investigaciones Energéticas, Medioambientales y Tecnológicas (CIEMAT), Madrid, Spain*
[29]*Department of Physics, Stanford University, 382 Via Pueblo Mall, Stanford, CA 94305, USA*
[30]*Department of Physics, IIT Hyderabad, Kandi, Telangana 502285, India*
[31]*Fermi National Accelerator Laboratory, P. O. Box 500, Batavia, IL 60510, USA*
[32]*Excellence Cluster Universe, Boltzmannstr. 2, 85748 Garching, Germany*
[33]*Faculty of Physics, Ludwig-Maximilians-Universität, Scheinerstr. 1, 81679 Munich, Germany*
[34]*Jet Propulsion Laboratory, California Institute of Technology, 4800 Oak Grove Dr., Pasadena, CA 91109, USA*

[35]*Department of Astronomy/Steward Observatory, 933 North Cherry Avenue, Tucson, AZ 85721-0065, USA*
[36]*Department of Astronomy, University of Michigan, Ann Arbor, MI 48109, USA*
[37]*Institute for Astronomy, University of Edinburgh, Edinburgh EH9 3HJ, UK*
[38]*Jet Propulsion Laboratory, California Institute of Technology, Pasadena, CA 91109, USA*
[39]*Department of Physics and Astronomy, University College London, Gower Street, London WC1E 6BT, UK*
[40]*Instituto de Fisica Teorica UAM/CSIC, Universidad Autonoma de Madrid, 28049 Madrid, Spain*
[41]*Universitäts-Sternwarte, Fakultät für Physik, Ludwig-Maximilians Universität München, Scheinerstr. 1, 81679 München, Germany*
[42]*Department of Physics, ETH Zurich, Wolfgang-Pauli-Strasse 16, CH-8093 Zurich, Switzerland*
[43]*Santa Cruz Institute for Particle Physics, Santa Cruz, CA 95064, USA*
[44]*Department of Physics, The Ohio State University, Columbus, OH 43210, USA*
[45]*Max Planck Institute for Extraterrestrial Physics, Giessenbachstrasse, 85748 Garching, Germany*
[46]*Lawrence Berkeley National Laboratory, 1 Cyclotron Road, Berkeley, CA 94720, USA*
[47]*Australian Astronomical Observatory, North Ryde, NSW 2113, Australia*
[48]*Departamento de Física Matemática, Instituto de Física,*
Universidade de São Paulo, CP 66318, São Paulo, SP, 05314-970, Brazil
[49]*George P. and Cynthia Woods Mitchell Institute for Fundamental Physics and Astronomy,*
and Department of Physics and Astronomy, Texas A&M University, College Station, TX 77843, USA
[50]*Department of Astronomy, The Ohio State University, Columbus, OH 43210, USA*
[51]*Institució Catalana de Recerca i Estudis Avançats, E-08010 Barcelona, Spain*
[52]*Department of Physics and Astronomy, Pevensey Building, University of Sussex, Brighton, BN1 9QH, UK*
[53]*ICTP South American Institute for Fundamental Research*
Instituto de Física Teórica, Universidade Estadual Paulista, São Paulo, Brazil
[54]*School of Physics and Astronomy, University of Southampton, Southampton, SO17 1BJ, UK*
[55]*Brandeis University, Physics Department, 415 South Street, Waltham MA 02453*
[56]*Instituto de Física Gleb Wataghin, Universidade Estadual de Campinas, 13083-859, Campinas, SP, Brazil*
[57]*Computer Science and Mathematics Division, Oak Ridge National Laboratory, Oak Ridge, TN 37831*

We present constraints on extensions of the minimal cosmological models dominated by dark matter and dark energy, ΛCDM and wCDM, by using a combined analysis of galaxy clustering and weak gravitational lensing from the first-year data of the Dark Energy Survey (DES Y1) in combination with external data. We consider four extensions of the minimal dark energy-dominated scenarios: 1) nonzero curvature Ω_k, 2) number of relativistic species $N_{\rm eff}$ different from the standard value of 3.046, 3) time-varying equation-of-state of dark energy described by the parameters w_0 and w_a (alternatively quoted by the values at the pivot redshift, w_p, and w_a), and 4) modified gravity described by the parameters μ_0 and Σ_0 that modify the metric potentials. We also consider external information from Planck cosmic microwave background measurements; baryon acoustic oscillation measurements from SDSS, 6dF, and BOSS; redshift-space distortion measurements from BOSS; and type Ia supernova information from the Pantheon compilation of datasets. Constraints on curvature and the number of relativistic species are dominated by the external data; when these are combined with DES Y1, we find $\Omega_k = 0.0020^{+0.0037}_{-0.0032}$ at the 68% confidence level, and the upper limit $N_{\rm eff} < 3.28\,(3.55)$ at 68% (95%) confidence, assuming a hard prior $N_{\rm eff} > 3.0$. For the time-varying equation-of-state, we find the pivot value $(w_p, w_a) = (-0.91^{+0.19}_{-0.23}, -0.57^{+0.93}_{-1.11})$ at pivot redshift $z_p = 0.27$ from DES alone, and $(w_p, w_a) = (-1.01^{+0.04}_{-0.04}, -0.28^{+0.37}_{-0.48})$ at $z_p = 0.20$ from DES Y1 combined with external data; in either case we find no evidence for the temporal variation of the equation of state. For modified gravity, we find the present-day value of the relevant parameters to be $\Sigma_0 = 0.43^{+0.28}_{-0.29}$ from DES Y1 alone, and $(\Sigma_0, \mu_0) = (0.06^{+0.08}_{-0.07}, -0.11^{+0.42}_{-0.46})$ from DES Y1 combined with external data. These modified-gravity constraints are consistent with predictions from general relativity.

I. INTRODUCTION

Evidence for dark matter [1] and the discovery of cosmic acceleration and thus evidence for dark energy [2, 3] were pinnacle achievements of cosmology in the 20th century. Yet because of the still-unknown physical mechanisms behind these two components, understanding them presents a grand challenge for the present-day generation of cosmologists. Dark matter presumably corresponds to an as-yet undiscovered elementary particle whose existence, along with couplings and other quantum properties, is yet to be confirmed and investigated. Dark energy is even more mysterious, as there are no compelling models aside, arguably, from the simplest one of vacuum energy.

Dark matter and dark energy leave numerous unambiguous imprints in the expansion rate of the universe and in the rate of growth of cosmic structures as a function of time. The theoretical modeling and direct measurements of these signatures have led to a renaissance in data-driven cosmology. Numerous ground- and space-based sky surveys have dramatically improved our census of dark matter and dark energy over the past two decades, and have led to a consensus model with $\sim$5% energy density in baryons, $\sim$25% in cold (non-relativistic) dark matter (CDM), and $\sim$70% in dark energy. These probes, reviewed in [4–6], include the cosmic microwave background (CMB; [7]); galaxy clustering including the location of the baryon acoustic oscillation (BAO) feature and the impact of redshift space distortions (RSD); distances to type Ia supernovae (SNe Ia); weak gravitational lensing (WL [8]), given

by tiny distortions in the shapes of galaxies due to the deflection of light by intervening large-scale structure; and the abundance of clusters of galaxies [9].

The simplest and best-known model for dark energy is the cosmological constant. This model, represented by a single parameter given by the magnitude of the cosmological constant, is currently in good agreement with data. On the one hand, vacuum energy density is predicted to exist in quantum field theory due to zero-point energy of quantum oscillators, and manifests itself as a cosmological constant: unchanging in time and spatially smooth. On the other hand, the theoretically expected vacuum energy density is tens of orders of magnitude larger than the observed value as has been known even prior to the discovery of the accelerating universe [10, 11]. Apart from the cosmological constant, there exists a rich set of other dark energy models including evolving scalar fields, modifications to general relativity, and other physically-motivated possibilities [12–14] with many possible avenues to test them with data [15]. Testing for such extensions of the simplest dark energy model on the present-day data has spawned an active research area in cosmology [16–32], and is the subject of the present paper.

The Dark Energy Survey (DES[1]) [33] is a photometric survey imaging the sky in five filters ($grizY$) using the 570 Mpixels, 3 deg^2 field-of-view Dark Energy Camera (DECam) [34], mounted on the 4-meter Blanco telescope at the Cerro Tololo International Observatory in Chile. After more than five years of data-taking, the survey will end in early 2019 with more than 300 million galaxies catalogued in an area of roughly 5000 deg^2.

In 2017 the DES collaboration published the analyses of its first year of data (Y1). It presented results which put constraints on certain cosmological parameters derived from their late-universe imprints in galaxy surveys at the same level of precision as the constraints obtained on these same parameters from their *early*-universe signatures in the CMB data. These results, described in [35] (hereafter Y1KP) are based on the two-point statistics of galaxy clustering and weak gravitational lensing. The combined analysis of the three different two-point correlation functions (galaxy clustering, cosmic shear, and the galaxy-shear cross-correlation, typically referred to as galaxy-galaxy lensing) is the end-product of a complex set of procedures which includes the analysis pipeline and methodology [36], its validation on realistic simulations [37], the creation of shape catalogs [38], the estimation and validation of the redshift distribution for different galaxy samples [39], measurement and derivation of cosmological constraints from the cosmic shear signal [40], galaxy–galaxy lensing results [41] and the galaxy clustering statistics [42]. Both alone and in combination with external data from CMB (Planck [43]), BAO (6dF Galaxy Survey [44], the SDSS Data Release 7 Main Galaxy Sample [45], BOSS Data Release 12 [46]) and SNe Ia (Joint Lightcurve Analysis (JLA [47]), DES provides precise measurements in the parameters

describing the amplitude of mass fluctuations perturbation and the matter energy density evaluated today. We refer the reader to Y1KP for more details of the DES Y1 analysis, and to Sec II D below for further description of external data.

In Y1KP we considered only the two simplest models for dark energy: the standard cosmological constant ΛCDM model and a wCDM model with an extra parameter (the dark energy equation-of-state w) accounting for a constant relation between the pressure and the energy density of the dark energy fluid ($p = w\rho$). In this paper we explore the impact of the DES Y1 data on the analysis of a few extensions of the standard flat ΛCDM and wCDM models considered in Y1KP, namely the possibilities of:

- Nonzero spatial curvature;

- New relativistic degrees of freedom;

- Time-variation of the dark energy equation-of-state;

- Modifications of the laws of gravity on cosmological scales.

We describe these extensions in more detail below.

Our analysis applies the same validation tests with respect to assumptions about the systematic biases, analysis choices, and pipeline accuracy, as previously done in Y1KP. We also adopt the parameter-level blinding procedure used in that paper, and we do not look at the final cosmological constraints until after unblinding, when the analysis procedure and estimates of uncertainties on various measurement and astrophysical nuisance parameters were frozen. Validation and parameter blinding are also described in further detail below.

Our study effectively complements and extends a number of studies of extensions to Λ/wCDM in the literature using state-of-the-art data, e.g. by Planck [25, 43], the Baryon Oscillation Spectroscopic Survey (BOSS) [46], the Kilo Degree Survey (KiDS) [28, 48] and more recently by using the Pantheon compilation of SNe Ia data [49]. These studies report no significant deviations from ΛCDM. We will comment on the comparison of our results to these existing constraints in the conclusions.

The paper is organized as follows: the data sets used in the analyses are described in §II, while the models and parameters used to describe the data are detailed in §III. To ensure that our analysis will not mis-attribute an astrophysical systematic error to a *detection* of an extension, we present a series of validation tests in §IV. In §V, we present our results before concluding in §VI.

II. DATA

The primary data used in this study are the auto- and cross-correlations of galaxy positions and shapes measured in data taken by the Dark Energy Survey during its first year of observations.[2] We refer the reader to Y1KP for details and only

---

---

give a summary here.

A. Catalogs

The images taken between August 31, 2013 and February 9, 2014 were processed with the DES Data Management (DESDM) system [50–53], and its outputs validated and filtered to produce the high-quality DES Y1 Gold catalog [54].

From the galaxies in this catalog, we define two samples to be used here: *lens* galaxies, for which we measure the angular correlation function of positions, and *source* galaxies, for which we measure the auto-correlation of shapes and the cross-correlation of shapes with lens galaxy positions. To reduce the impact of varying survey characteristics and to remove foreground objects and contaminated regions, we define both samples over an area of 1321 deg^2.

As *lens* galaxies, we use a sample of luminous red galaxies identified with the REDMAGIC algorithm [55]. This choice is motivated by the small uncertainties in photometric redshifts, high completeness over most of our survey, and the strong clustering of these galaxies. We divide the REDMAGIC sample into five redshift bins, using three different cuts on intrinsic luminosity to ensure completeness. For bins of redshift $z \in [(0.15 - 0.3), (0.3 - 0.45), (0.45 - 0.6)]$, we chose a luminosity cut of $L > 0.5L_*$ with a spatial density $\bar{n} = 10^{-3}(h^{-1}\mathrm{Mpc})^{-3}$, where the comoving density assumes a fiducial ΛCDM cosmology. For the additional redshift bins $z \in (0.6 - 0.75)$ and $(0.75 - 0.9)$, the luminosity cuts and densities are $L > L_*, \bar{n} = 4 \times 10^{-4}(h^{-1}\mathrm{Mpc})^{-3}$ and $L > 1.5L_*$, $\bar{n} = 10^{-4}(h^{-1}\mathrm{Mpc})^{-3}$, respectively. In total, these samples contain approximately 660,000 lens galaxies.

The primary systematic uncertainties in this catalog are based on residual correlations of galaxy density with observational characteristics of the survey, and in the uncertainty and bias of the lens galaxy redshifts as estimated from the broad-band photometry. The first effect is studied in detail and corrected in [42]. The redshift distributions estimated for the REDMAGIC galaxies are validated, and the budget for residual uncertainties in quantified, using their clustering with spectroscopic galaxy samples [56].

To generate a catalog of *source* galaxies with accurate shapes for estimating lensing signals, we use the METACALIBRATION method [57, 58] on top of NGMIX[3]. NGMIX provides the ellipticity measurements for a sufficiently resolved and high signal-to-noise subsample of the Y1 Gold catalog by fitting a simple Gaussian mixture model, convolved with the individual point spread function, to the set of all single exposures taken of a galaxy. The primary systematic uncertainty in this catalog is a multiplicative error on the mean shear measurement due to biases related to noise and selection effects. In the METACALIBRATION scheme, this bias is removed by introducing an artificial shear signal and measuring the *response* of the mean measured ellipticity to the introduced shear. To
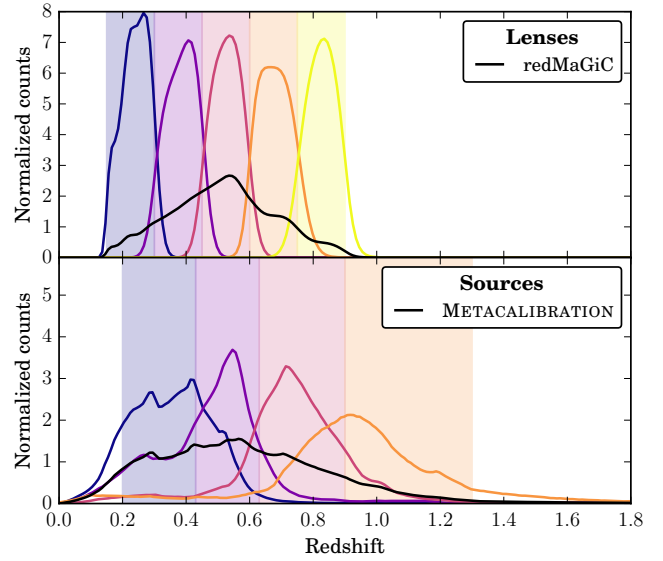

FIG. 1. Estimated redshift distributions of the lens and source galaxies used in the analysis. The shaded vertical regions define the bins: galaxies are placed in the bin spanning their mean photo-z estimate. We show both the redshift distributions of galaxies in each bin (colored lines) and their overall redshift distributions (black lines).

this end, all galaxy images are artificially sheared, and their ellipticities and all properties used for selecting the sample are re-measured on the sheared versions of their images. By applying a response correction to all estimated shear signals, we find that this method provides measurements with a small multiplicative bias that is dominated by the effect of blending between neighboring galaxies [38].

To divide these source galaxies into redshift bins, we use the means of the redshift probability distributions provided by a version of the BPZ algorithm [59]. This procedure is based on the METACALIBRATION measurements of $griz$ galaxy fluxes, as detailed in [39]. By splitting on $z_{\mathrm{mean}} \in [(0.2 - 0.43), (0.43 - 0.63), (0.63 - 0.9), (0.9 - 1.3)]$, we generate four bins with approximately equal density. The redshift distribution of each source bin is initially estimated from the stack of individual galaxy BPZ redshift probability distributions. This initial estimate is validated, and the systematic uncertainty on the mean redshift in each bin is estimated using a resampling method of high-quality photometric redshifts gained from multi-band data in COSMOS [39] and the clustering of the sources with REDMAGIC galaxies [60, 61].

The lens and source galaxy distributions are shown in Figure 1. The systematic uncertainties on redshift of both samples, and on the shear estimates of the source sample, are quantified in [38, 39] and marginalized over in all cosmological likelihoods.

---

[3] https://github.com/esheldon/ngmix

B. Measurements

For the lens and source sample, we use measurements of the three sets of two-point functions in [35]:

- *Galaxy clustering*: the auto-correlation of lens galaxy positions in each redshift bin $w(\theta)$, i.e. the fractional excess number of galaxy pairs of separation θ relative to the number of pairs of randomly distributed points within our survey mask [42],

- *Cosmic shear*: the auto-correlation of source galaxy shapes within and between the source redshift bins, of which there are two components $\xi_\pm(\theta)$, taking the products of the ellipticity components of pairs of galaxies, either adding ($+$) or subtracting ($-$) the component tangential to the line connecting the galaxies and the component rotated by $\pi/4$ [40],

- *Galaxy-galaxy lensing*: the mean tangential ellipticity of source galaxy shapes around lens galaxy positions, for each pair of redshift bins, $\gamma_t(\theta)$ [41].

Details of these measurements and the checks for potential systematic effects in them are described in detail in [40–42], and an overview of the full data vector is given in [35]. Here we follow Y1KP, and refer to results from combining all 3 two-point functions as "DES Y1 3×2pt".

Each of these measurements is performed in a set of 20 logarithmic bins of angular separation between 2.5' and 250' using the software TREECORR [62]. We only use a subset of these bins, removing small scales on which our model is not sufficiently accurate. The fiducial scales that we use for clustering and galaxy-galaxy lensing correspond to minimal scale of $R = 8 \, h^{-1} \mathrm{Mpc}$ and $12 \, h^{-1} \mathrm{Mpc}$, respectively. For cosmic shear, the minimal angular scale $\theta_{\min}$ is redshift-dependent, and is determined by requiring that the cross-correlation $(\xi_\pm)_{ij}(\theta_{\min})$ at a pair of redshift bins i and j not incur an expected fractional contribution from baryonic interactions exceeding 2%; see [40] for details.

For the curvature, number of relativistic species, and dark energy tests, we use the exact same set of scales as in Y1KP, and the datavector with a total of 457 measurements in $(w(\theta), \xi_\pm(\theta), \gamma_t(\theta))$. For our modified gravity tests, we use a more stringent range of scales, described at the end of Sec. III C 4; this datavector spans only the linear scales, and has a total of 334 measurements.

DES Y1 measurements provide information at $z \lesssim 1$, when – in most models – dark energy starts to play a role in cosmic evolution. They provide information about both the geometrical measures (distances, volumes) and the growth of cosmic structure. In particular, both lensing and galaxy clustering are sensitive to the growth of structure, while the kernels in the calculation of the corresponding two-point correlation functions also encode the geometry given by distances (see e.g. equations in Sec. 4 of Y1KP). Therefore, all of the DES Y1 3×2pt measurements probe both geometry and the growth of structure, and thus complement the largely geometrical external data discussed below in Sec. II D. The geometry-plus-growth aspect of the DES Y1 3×2pt measurements makes them particularly sensitive to predictions of the models studied in this paper such as modified gravity.

C. Covariance

The statistical uncertainties of these measurements are due to spatial variations in the realizations of the cosmic matter density field (cosmic variance) and random processes governing the positions (shot noise) and intrinsic orientations (shape noise) of galaxies. We describe these uncertainties and their correlations with a covariance matrix $\mathbf{C}$, which is calculated using CosmoLike [63] using the relevant four-point functions in the halo model [64]. Shot and shape noise are scaled according to the actual number of source galaxies in our radial bins to account for source clustering and survey geometry. Details of this approach are described in [63, 65], along with our validation of the covariance matrix and the corresponding Gaussian likelihood.

D. External data

Combining the DES large-scale structure weak lensing and galaxy clustering data with other, independent probes has benefits in constraining the beyond-minimal cosmological models considered in this paper. In particular, the measurements of distances by SNe Ia and BAO, along with the distance to recombination from the CMB, provide precise geometrical measures, while redshift-space distortions (RSD) are sensitive to the growth of cosmic structure [66–70]. These external data significantly complement the combination of geometry and growth probed by the DES clustering and lensing data. Similarly, combining DES with external data enables the comparison of the inferred cosmology from early- and late-time probes (see e.g. Fig. 11 in Y1KP).

As in Y1KP, we combine DES data with a collection of external data sets to derive the most precise constraints on the ΛCDM extensions models. We use CMB, CMB Lensing, BAO, RSD, and Supernova Ia measurements in various combinations. Our final set of external data, described in more detail below, is similar to that used in Y1KP; the main differences are that we add RSD measurements from BOSS, and that we update the JLA supernova dataset used in Y1KP to the more recent Pantheon results.

We treat the likelihoods of individual external datasets as independent, simply summing their log-likelihoods. We now describe the individual external datasets that we add to DES data in our combined analysis.

1. CMB & CMB lensing

The cosmic microwave background temperature T and polarization (E- and B-modes) anisotropies are a powerful probe of the early universe. The combination of a rich phenomenology with linear perturbations to a background yields

very strong constraints on density perturbations in the early Universe, and on reionization.

In this work we use the Planck 2015 likelihood[4] as described in Aghanim *et al.* [71]. We use the Planck TT likelihood for multipoles $30 \leq \ell \leq 2508$ and the joint TT, EE, BB and TE likelihood for $2 \leq \ell \leq 30$. We refer to this likelihood combination as TT+lowP.[5]

Planck primary CMB measurements like these strongly constrain all of the baseline cosmological parameters that we use across our models. They have varying power to constrain extension parameters.

We also make use of Planck CMB lensing measurements [72], from temperature only[6]. These are measured from higher-order correlations in the temperature field, and act like an additional narrow and very high redshift source sample. We neglect any cross-correlation between DES Y1 measurements and Planck's CMB lensing map because 1) the noise in the CMB lensing map is sufficiently large; 2) the overlap of the surveys is small compared to the total CMB lensing area; and 3) the CMB lensing auto-spectrum receives most of its contribution from $z \simeq 2$, while DES constraints are at $z \lesssim 1$, which further reduces covariance. We have explicitly tested that the assumption of ignoring the DES-CMBlens covariance holds to an excellent accuracy.

2. BAO + RSD

BAO measurements locate a peak in the correlation function of cosmic structure that corresponds to the sound horizon at the drag epoch. Since the sound speed before that point depends only on the well-understood ratio of photon to baryon density, this horizon acts as a standard ruler and can be used to measure the angular diameter distance with a percent-level precision.

As in Y1KP we use BAO measurements from BOSS Data Release 12 [46], which provides measurements of both the Hubble parameter $H(z_i)$ and the comoving angular diameter distance $d_A(z_i)$, at three separate redshifts, $z_i = \{0.38, 0.51, 0.61\}$. The other two BAO data that we use, 6DF Galaxy survey [44] and SDSS Data Release 7 Main Galaxy Sample [45], are lower signal-to-noise and can only tightly constrain the spherically averaged combination of transverse and radial BAO modes, $D_V(z) \equiv [cz(1 + z)^2 D_A^2(z)/H(z)]^{1/3}$. These constraints are at respective redshifts $z = 0.106$ (6dF) and $z = 0.15$ (SDSS MGS).

We also utilize the redshift-space distortion measurements from BOSS DR12; they are given as measurements of the

quantity $f(z_i)\sigma_8(z_i)$ at the aforementioned three redshifts. Here f is the linear growth rate of matter perturbations and σ_8 is the amplitude of mass fluctuations on scales $8\,h^{-1}\mathrm{Mpc}$. We employ the full covariance, given by [46], between these three RSD measurements and those of BAO quantities $H(z_i)$ and $d_A(z_i)$. We treat the 6dF and SDSS MGS measurements as independent of those from BOSS DR12, and we neglect any cosmological dependence on the derived values of $f(z_i)\sigma_8(z_i)$ from BOSS DR12 data.

Finally, we ignore the covariance between these BAO/RSD measurements and those of DES galaxy clustering and weak lensing; the two sets of measurements are carried out on different areas on the sky and the covariance is expected to be negligible.

3. Supernovae

Type Ia supernovae (SNe Ia) provide luminosity distances out to redshift of order unity and beyond, and thus excellent constraints on the expansion history of the universe. In this analysis we use the Pantheon SNe Ia sample [49] which combines 279 SNe Ia from the Pan-STARRS1 Medium Deep Survey ($0.03 < z < 0.68$) with SNe Ia from SDSS, SNLS, various low-z and HST samples. The Pantheon data was produced using the Pan-STARRS1 Supercal algorithm [73] which established global calibration for 13 different SNe Ia samples. The final Pantheon sample includes 1048 objects in the redshift range $0.01 < z < 2.26$.

III. THEORY AND MODELING

A. Standard cosmological parameters

We assume the same set of ΛCDM cosmological parameters described in Y1KP, then supplement it with parameters alternately describing four extensions. We parametrize the matter energy density today relative to the critical density Ω_m, as well as that of the baryons Ω_b and of neutrinos Ω_ν[7]. Moreover, we adopt the amplitude A_s and the scalar index n_s of the primordial density perturbations power spectrum, as well as the optical depth to reionization τ, and the value of the Hubble parameter today H_0. Except in the case of varying curvature, we assume that the universe is flat and, except in the case of varying dark energy, we assume that it is Λ-dominated with $w = -1$; under those two assumptions, $\Omega_\Lambda = 1 - \Omega_m$. Note that the amplitude of mass fluctuations σ_8 is a derived parameter, as is the parameter that decorrelates σ_8 and Ω_m, $S_8 \equiv \sigma_8(\Omega_m/0.3)^{0.5}$. The fiducial parameter set is therefore

$$\theta_{\text{base}} = \{\Omega_m, H_0, \Omega_b, n_s, A_s, (\tau)\}, \tag{1}$$

---

[4] Planck 2018 results [32] were released as this paper was in advanced stages of the analysis, so we stick with using the Planck 2015 likelihood. The main difference between the two is better measurements of CMB polarization in Planck 2018, resulting in better constraints on the optical depth τ.

[5] We used the public Planck likelihood files PLIK_LITE_V18_TT.CLIK and LOWL_SMW_70_DX11D_2014_10_03_V5C_AP.CLIK.

[6] We use the file SMICA_G30_FTL_FULL_PTTPTT.CLIK_LENSING.

---

[7] In the Σ_0, μ_0 systematic tests that use the older MGCAMB, this was not implemented, so Ω_ν is fixed in these tests. We do vary Ω_ν in our runs on the real data.

where the parentheses around the optical depth parameter indicate that it is used only in the analysis combinations that use CMB data.

To model the fully nonlinear power spectrum, we first estimate the linear primordial power spectrum on a grid of (k, z) using CAMB [74] or CLASS [75]. We then apply the HALOFIT prescription [76–78] to get the nonlinear spectrum. Throughout this work, we employ the version from Takahashi et al. [77].

In addition to this set of ΛCDM parameters, we use the following parametrization for each of the extension models:

1. Spatial curvature: Ω_k;

2. The effective number of neutrinos species N_{eff};

3. Time-varying equation-of-state of dark energy: w_0, w_a;

4. Tests of gravity: $\Sigma(a), \mu(a)$.

We describe these extensions in more detail below in Sec. III C.

B. Nuisance parameters

We follow the analysis in Y1KP, and model a variety of systematic uncertainties using an additional 20 nuisance parameters. The nuisance parameters are:

- Five parameters b_i that model linear bias of lens galaxies in five redshift bins;

- Two parameters, A_{IA} and η_{IA}, that model the power spectrum of intrinsic alignments as a power-law scaling $A_{\text{IA}}(\frac{1+z}{1+z_0})^{\eta_{\text{IA}}}$, with $z_0 = 0.62$ (see Sec. VIIB of [40] for a complete description of the model);

- Five parameters Δz_l^i to model the uncertainty in the means of distributions $n(z_i)$ of galaxies in each of the lens bins;

- Four parameters Δz_s^i to model the uncertainty in the means of distributions $n(z_i)$ of galaxies in each of the source bins;

- Four parameters m_i that model the overall uncertainty in the multiplicative shear bias in each of the source bins.

All of the cosmological and nuisance parameters in our standard analysis, along with their respective priors, are given in Table I.

Note that we did not change any assumptions about the nuisance parameters relative to our previous analysis applied to ΛCDM and wCDM. It is possible in principle that extensions (e.g. modified gravity) to these simplest models warrant more complicated modeling and therefore more nuisance parameters (e.g. adopting more complicated parametrizations of galaxy bias). To address this possibility, we consider a number of more complicated parametrizations of the systematic effects (described in Sec. IV) with the aim of determining

TABLE I. Parameters and priors used to describe the measured two-point functions, as adopted from Y1KP. *Flat* denotes a flat prior in the range given while *Gauss*(μ, σ) is a Gaussian prior with mean μ and width σ.

Parameter	Prior
Cosmology	
Ω_m	flat $(0.1, 0.9)$
A_s	flat $(5 \times 10^{-10}, 5 \times 10^{-9})$
n_s	flat $(0.87, 1.07)$
Ω_b	flat $(0.03, 0.07)$
h	flat $(0.55, 0.91)$
$\Omega_\nu h^2$	flat $(5 \times 10^{-4}, 10^{-2})$
Lens Galaxy Bias	
$b_i (i = 1, 5)$	flat $(0.8, 3.0)$
Intrinsic Alignment	
$A_{\text{IA}}(z) = A_{\text{IA}}[(1+z)/1.62]^{\eta_{\text{IA}}}$	
A_{IA}	flat $(-5, 5)$
η_{IA}	flat $(-5, 5)$
Lens photo-z shift (red sequence)	
Δz_l^1	Gauss $(0.008, 0.007)$
Δz_l^2	Gauss $(-0.005, 0.007)$
Δz_l^3	Gauss $(0.006, 0.006)$
Δz_l^4	Gauss $(0.000, 0.010)$
Δz_l^5	Gauss $(0.000, 0.010)$
Source photo-z shift	
Δz_s^1	Gauss $(-0.001, 0.016)$
Δz_s^2	Gauss $(-0.019, 0.013)$
Δz_s^3	Gauss $(+0.009, 0.011)$
Δz_s^4	Gauss $(-0.018, 0.022)$
Shear calibration	
$m_{\text{METACALIBRATION}}^i (i = 1, 4)$	Gauss $(0.012, 0.023)$

whether we could mis-identify a systematic effect as evidence for an extension. Our tests, also described in that section, indicate that constraints on the key extension parameters studied in this paper are not sensitive to these additional parameters. This justifies our choice not to modify our fiducial nuisance parameterization described in the bullet-point list above and used previously in Y1KP. Future, more precise data will require revisiting these, in addition to potentially extracting information about these extensions from the modified behavior of astrophysical nuisance effects.

C. ΛCDM extensions

We now introduce the four extensions to the simplest Λ/wCDM models that we study in this paper. The cosmological parameters describing these extensions, along with priors given to them in our analysis, are given in Table II.

1. Spatial Curvature

Standard slow-roll inflation predicts that spatial curvature is rapidly driven to zero. In this scenario, the amount of curvature expected today is $\Omega_k \simeq 10^{-4}$, where the tiny deviation from zero is expected from horizon-scale perturbations but will be very challenging to measure even with future cosmological data [79]. Departures from near-zero curvature are however expected in false-vacuum inflation, as well as scenarios that give rise to bubble collisions [80, 81]. With curvature, and ignoring the radiation density whose contribution is negligible in the late universe, the Hubble parameter generalizes to

$$\frac{H(a)}{H_0} = \left[\Omega_m a^{-3} + (1 - \Omega_m - \Omega_k) + \Omega_k a^{-2}\right]^{1/2}. \quad (2)$$

so that $\Omega_k < 0$ corresponds to spatially positive curvature, and the opposite sign to the spatially negative case. In this work, we compare constraints on Ω_k using DES data alone, as well as with combinations of subsets of the external data described in §II D.

We do not modify the standard HALOFIT prescription [76, 77] for prediction of the nonlinear power spectrum for nonzero values of Ω_k. Simulation measurements of the nonlinear spectrum for nonzero values of Ω_k do not exist to sufficiently validate this regime. However, it is not an unreasonable a priori assumption that the nonlinear modification to the power spectrum is only weakly affected by curvature beyond the primary effect captured in the linear power spectrum being modified. We do incorporate the impact of Ω_k in the evolution of the expansion and growth, which is properly modeled as part of the linear matter power spectrum that is modified by HALOFIT. We verify that this approximation does not significantly impact our results by comparing to the case where we restrict our data to scales that are safely 'linear' as described in §IV below.

2. Extra relativistic particle species

Anisotropies in the CMB are sensitive to the number of relativistic particle species. The Standard Model of particle physics predicts that the three left-handed neutrinos were thermally produced in the early universe and their abundance can be determined from the measured abundance of photons in the cosmic microwave background. If the neutrinos decoupled completely from the electromagnetic plasma before electron-positron annihilation, then the abundance of the three neutrino species today would be

$$n = N_{\text{eff}} \times 113 \, \text{cm}^{-3} \quad (3)$$

with $N_{\text{eff}} = 3$. In actuality, the neutrinos were slightly coupled during $e^{\pm}$ annihilation, so $N_{\text{eff}} = 3.046$ in the standard model [82–84]. Values of N_{eff} larger than this would point to extra relativistic species. The DES observations are less sensitive to N_{eff} than the CMB, because the effect of this parameter in the DES mainly appears via the change in the epoch of matter-radiation equality. Nevertheless, DES might constrain some parameters that are degenerate with N_{eff} so, at least in principle, adding DES observations to other data sets might provide tighter constraints.

There are well-motivated reasons for exploring possibilities beyond the standard scenario. First, the most elegant way to obtain small neutrino masses is the see-saw model [85], which typically relies on three new heavy Standard Model singlets, or sterile neutrinos. While these often are unstable and have very large masses, it is conceivable that sterile neutrinos are light and stable on cosmological time scales [86]. Indeed, there are a variety of experimental anomalies that could be resolved with the introduction of light sterile neutrinos, and a keV sterile neutrino remains an interesting dark matter candidate. If one or more light sterile neutrinos do exist, then they would typically be produced in the early universe via oscillations from the thermalized active neutrinos with an abundance determined by the mixing angles. As an example, the LSND/Miniboone anomaly [87, 88] could be resolved with a light sterile neutrino thus implying $N_{\text{eff}} \simeq 4$; the mixing angle of the sterile neutrino would dictate that it would have the same abundance as the 3 active neutrinos. More generally, a wide variety of extensions to the Standard Model contain light stable particles that would have been produced in the early Universe [89] and impacted the value of N_{eff}. It is important to note that while the addition of an extra relativistic species would explain some aspects of these observations, it is difficult for such models to accommodate all of the existing neutrino oscillation observations.

In the fiducial model, we are allowing for a single free parameter $\sum m_\nu$, treating the 3 active neutrinos as degenerate (since they would be approximately degenerate if they had masses in the range we can probe, > 0.1 eV). There is some freedom in how to parametrize the extension of a light sterile neutrino, however. If we attempt to model the addition of a single sterile neutrino, then in principle two new parameters must be added. For example, if the sterile neutrino has the same temperature as the active neutrinos, then the parameters can be chosen to be N_{eff}, allowed to vary between 3.046 and 4.046, and m_s, the mass of the sterile neutrino. Two light sterile neutrinos would require two more parameters, etc. However, we expect that the cosmological signal will be sensitive primarily to the total neutrino mass density and the number of effective massless species at the time of decoupling, as captured by N_{eff}, so we use only these two parameters, $\sum m_\nu$ and N_{eff}. Note that a value of N_{eff} appreciably different than 3 would point to a sterile neutrino or another light degree of freedom. We give N_{eff} a flat prior in the range $[3.0, 9.0]$, where the lower hard bound encodes the guaranteed presence of at least three relativistic neutrino species.

When varying N_{eff}, the fraction of baryonic mass in helium Y_p is set by a fitting formula based on the PArthENoPE BBN code [90]. This interpolates a Y_p for a given combination of $\Omega_b h^2$ and N_{eff}. An additional prior of $\Omega_b h^2 < 0.04$ is applied in the N_{eff} analysis to restrict the interpolation to its valid range.

3. Time-varying equation-of-state of dark energy

Given the lack of understanding of the physical mechanism behind the accelerating universe, it is important to investigate whether the data prefer models beyond the simplest one, the cosmological constant. In Y1KP, we investigated the evidence for a constant equation-of-state parameter $w \neq -1$. We found no evidence for $w \neq -1$, with a very tight constraint from the combination of DES Y1, CMB, SNe Ia, and BAO of $w = -1.00^{+0.05}_{-0.04}$.

We now investigate whether there is evidence for the time-evolution of the equation-of-state w. We consider the phenomenological model that describes dynamical dark energy [91]

$$w(a) = w_0 + (1 - a)w_a, \qquad (4)$$

where w_0 is the equation-of-state today, while w_a is its variation with scale factor a. The (w_0, w_a) parametrization fits many scalar field and some modified gravity expansion histories up to a sufficiently high redshift, and has been used extensively in past constraints on dynamical dark energy.

It is also useful to quote the value of the equation-of-state at the pivot $w_p \equiv w(a_p)$; this is the scale factor at which the equation-of-state value and its variation with the scale factor are decorrelated, and where $w(a)$ is best-determined. Rewriting Eq. (4) as $w(a) = w_p + (a_p - a)w_a$, the pivot scale factor is

$$a_p = 1 + \frac{\mathbf{C}_{w_0 w_a}}{\mathbf{C}_{w_a w_a}} \qquad (5)$$

where $\mathbf{C}$ is the parameter covariance matrix in the 2D (w_0, w_a) space, obtained by marginalizing the full 28×28 covariance over the remaining 26 parameters. The corresponding pivot redshift is of course $z_p = 1/a_p - 1$.

The linear-theory observable quantities in this model are straightforwardly computed, as the new parameters affect the background evolution in a known way, given that the Hubble parameter becomes

$$\frac{H(a)}{H_0} = \left[\Omega_m a^{-3} + (1 - \Omega_m) a^{-3(1+w_0+w_a)} e^{-3w_a(1-a)} \right]^{1/2} . \qquad (6)$$

To obtain the nonlinear clustering in the (w_0, w_a) model, we assume the same linear-to-nonlinear mapping as in the ΛCDM model, except for the modified expansion rate $H(z)$ [92–94]. In particular, we implement the same HALOFIT nonlinear [76, 77] prescription as we do in the fiducial ΛCDM case. We impose a hard prior $w_0 + w_a \leq 0$; models lying in the forbidden region have a positive equation of state in the early universe, are typically ruled out by data, and would present additional challenges in numerical calculations. For the same reason we impose the prior $w_0 < -0.33$. Note also that in our analysis we do implicitly allow the "phantom" models where $w(a) < -1$; while not a feature of the simplest physical models of dark energy (e.g. single-field quintessence), such a violation of the weak energy condition is in general allowed [95].

TABLE II. Summary of the extensions to the ΛCDM model that we study in this paper, the parameters that describe these extensions, and the (flat) priors given to these parameters. In addition to the priors listed in the table, we also impose the prior $w_0 + w_a \leq 0$ for dark energy, and $2\Sigma_0 + 1 > \mu_0$ for modified gravity.

ΛCDM Extension	Parameter	Flat Prior
Curvature	Ω_k	$[-0.25, 0.25]$
Number relativistic species	N_{eff}	$[3.0, 7.0]$
Dynamical dark energy	w_0	$[-2.0, -0.33]$
	w_a	$[-3.0, 3.0]$
Modified gravity	Σ_0	$[-3.0, 3.0]$
	μ_0	$[-3.0, 3.0]$

4. Modified gravity

The possibility of deviations from General Relativity on cosmological scales has been motivated by the prospect that an alternative theory of gravity could offer an explanation for the accelerated expansion of the Universe. In the past several years, numerous works constraining modifications to gravity using cosmological data have been published, including from the Planck team [25, 32], the Kilo Degree Survey [28], and the Canada-France-Hawaii Lensing Survey [96]. Constraints from the Dark Energy Survey Science Verification data were obtained in [97]. Recently, stringent constraints were made on certain alternative theories of gravity [98–104] via the simultaneous observation of gravitational and electromagnetic radiation from a binary neutron star merger with the Laser Interferometer Gravitational Wave Observatory (LIGO) [105].

In what follows, we refer to the scalar-perturbed Friedmann-Robertson-Walker line element in the conformal Newtonian gauge:

$$ds^2 = a^2(\tau) \left[(1 + 2\Psi)d\tau^2 - (1 - 2\Phi)\delta_{ij}dx_i dx_j \right] . \qquad (7)$$

In General Relativity and without anisotropic stresses, $\Psi = \Phi$. The parameterization of deviations from General Relativity studied in this work is motivated by theoretical descriptions which make use of the quasistatic approximation (see, e.g., [106]). It can be shown that in the regime where linear theory holds and where it is a good approximation to neglect time derivatives of novel degrees of freedom (e.g. extra scalar fields), the behavior of the majority of cosmologically-motivated theories of gravity can be summarized via a free function of time and scale multiplying the Poisson equation, and another which represents the ratio between the potentials Φ and Ψ. Such a parameterization is an effective description of a more complicated set of field equations [107–116], but this approximation has been numerically verified on scales relevant to our present work [117–121].

There are a number of related pairs of functions of time and scale which can be used in a quasistatic parameterization of gravity; we choose the functions μ and Σ, defined as

$$k^2\Psi = -4\pi Ga^2(1 + \mu(a))\rho\delta\,, \qquad (8)$$

$$k^2(\Psi + \Phi) = -8\pi Ga^2(1 + \Sigma(a))\rho\delta\,, \qquad (9)$$

where we are working in Fourier space where k is the wavenumber, and δ is the comoving-gauge density perturbation. This version of the parameterization was used in [25, 32, 96], and benefits from the fact that Σ parametrizes the change in the lensing response of massless particles to a given matter field, while μ is linked to the change in the matter overdensity itself. Therefore, weak lensing measurements are primarily sensitive to Σ but also have some smaller degree of sensitivity to μ via their tracing of the matter field, whereas galaxy clustering measurements depend only on μ and are insensitive to Σ. We find the DES data alone are more sensitive to Σ than to μ; constraining the latter requires combining DES with a non-relativistic tracer of large-scale structure such as the RSD (e.g. [96, 97]) which we also do below as part of our combined analysis.

To practically constrain μ and Σ, we select a functional form of

$$\mu(z) = \mu_0\frac{\Omega_\Lambda(z)}{\Omega_\Lambda}\,, \quad \Sigma(z) = \Sigma_0\frac{\Omega_\Lambda(z)}{\Omega_\Lambda} \qquad (10)$$

where $\Omega_\Lambda(z)$ is the redshift-dependent dark energy density (in the ΛCDM model) relative to critical density, and Ω_Λ is its value today. This time dependence has been introduced in [122], and is widely employed (see e.g. [25, 32, 96]). It is motivated by the fact that in order for modifications to GR to offer an explanation for the accelerated expansion of the Universe, we would expect such modifications to become significant at the same timescale as the acceleration begins. We do not model any scale-dependence of μ and Σ since it has been shown to be poorly constrained by current cosmological data while not much improving the goodness-of-fit [25]. We therefore include only the parameters μ_0 and Σ_0 (but, as explained in Sec. IV A, only quote constraints on Σ_0). In GR, $\mu_0 = \Sigma_0 = 0$.

Note that although our choice of parameterization is motivated by the quasistatic limit of particular theories of gravity, our analysis takes an approach which is completely divorced from any given theory. We endeavor instead to make empirical constraints on the parameters μ_0 and Σ_0 as specified by Eqs. (8), (9), and (10). Because we take this empirically-driven approach, we include certain data elements in which the quasistatic approximation would not be expected to hold, most importantly the near-horizon scales for the ISW effect. Although not rigorously theoretically justified, a similar approach with respect to inclusion of the ISW effect at large scales was taken in, for example, [96]. Practically, this choice has the benefit of providing an important constraint on τ from external CMB data, which is useful in breaking degeneracies.

We use CosmoSIS with a version of MGCamb[8] [123, 124]

—————

modified to include the Σ, μ parametrization to compute the linear matter power spectrum and the CMB angular power spectra. For some sets of (Σ_0, μ_0) MGCamb returns an error; we estimated this region of parameter space can be avoided by imposing an additional hard prior $\mu_0 < 1 + 2\Sigma_0$. We therefore implement this prior in order to avoid computations for parameters not handled by MGCamb. The effects of this hard prior can be visually observed in our constraints on modified-gravity parameters with DES alone (Fig. 4 below); we demostrate in Appendix A that its effects on the combined DES+external constraint is likely to be minimal.

To validate our modified-gravity analysis pipeline, we compare the CosmoSIS results to that of another code, CosmoLike [63]. We require that the two codes give the same theory predictions for clustering and lensing observables, and the same constraints on cosmological parameters given a synthetic data vector. The comparison shows good agreement, and details can be found in Appendix A.

Finally, because the (μ, Σ) description does not constitute a complete theoretical model, its nonlinear clustering predictions are not available to us even in principle. We therefore restrict ourselves to the linear-only analysis. To do this, we follow the Planck 2015 analysis [25] and consider the difference between the nonlinear and linear-theory predictions in the standard ΛCDM model at best-fit values of cosmological parameters and with no modified gravity. Using the respective data vector theory predictions, $\mathbf{d}_{\mathrm{NL}}$ and $\mathbf{d}_{\mathrm{lin}}$, and full error covariance of DES Y1, $\mathbf{C}$, we calculate the quantity

$$\Delta\chi^2 \equiv (\mathbf{d}_{\mathrm{NL}} - \mathbf{d}_{\mathrm{lin}})^T\,\mathbf{C}^{-1}\,(\mathbf{d}_{\mathrm{NL}} - \mathbf{d}_{\mathrm{lin}}) \qquad (11)$$

and identify the single data point that contributes most to this quantity. We remove that data point, and repeat the process until $\Delta\chi^2 < 1$. The resulting set of 334 (compared to the original 457) data points that remain constitutes our fiducial choice of linear-only scales.

IV. VALIDATION TESTS AND BLINDING

We subject our ΛCDM extensions analyses to the same battery of tests for the impact of systematics as in Y1KP. The principal goal is to ensure that all of our analyses are robust with respect to the effect of reasonable extensions to models of astrophysical systematics and approximations in our modeling. As part of the same battery of tests, we also test that the range of spatial scales that are used lead to unbiased cosmological results, and that motivated modifications to our modeling assumptions do not significantly change the inferred cosmology.

In these tests and the results below,[9] sampling of the posterior distribution of the parameter space is performed

—————
[9] One important distinction from the data-based results in later sections is that we sample a lower-precision version of the CMB lensing contribution to constraints including external data when varying Ω_k, then modify the posterior to the higher precision prediction via importance sampling. We do this to speed up the evaluation of non-flat models, as in our implementa-
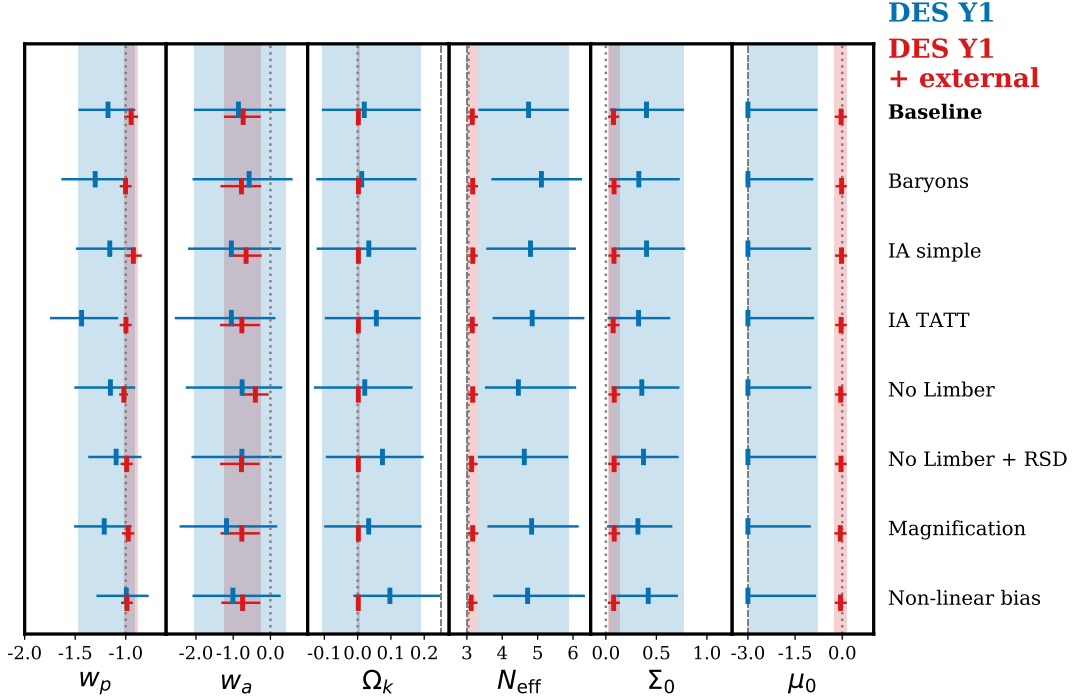
FIG. 2. Impact of assumptions and approximations adopted in our analysis, demonstrated on synthetic data (that is, noiseless DES data centered on the theoretical expectation, along with actual external data). Each column shows one of the cosmological parameters describing ΛCDM extensions; the dotted vertical line is the true input value of that parameter in the DES data vector (which does not necessarily coincide with the parameter values preferred by the external data). The vertical shaded bands show the marginalized 68% CL constraints in the baseline model for the DES-only synthetic data (blue) and DES+external. The horizontal error bars show the inferred constraint for each individual addition to the synthetic data vector which are listed in rows; they match the shaded bands for the baseline case. For subsequent rows, they show the inferred constraint for each individual addition to the synthetic data vector as listed on the right. Some cases that appear inconsistent with the baseline analysis are discussed further in Sec. IV A. In cases where the prior is informative, we also include a dashed vertical line to signify the prior edge.

with `Multinest` [125] and `emcee` [126] wrappers within `CosmoSIS`[10] [127] and `CosmoLike` [63]. While the convergence of `Multinest` is intrinsic to the sampler and achieved by verifying that the uncertainty in the Bayesian evidence is below than some desired tolerance, we explicitly check the convergence of `emcee` chains. In order to do so, we compute the autocorrelation length of each walk, then continue the walks until a large number of such lengths is reached[11]. The autocorrelation length estimates how long a chain needs to be in order for new "steps" to be uncorrelated with previous ones. We then split chains into several uncorrelated segments and verify that marginalized parameter constraints do not change significantly when these segments are compared with each other. The typical number of samples of the posterior in these chains is between two and three million. We

have also verified in select cases that this procedure leads to excellent agreement with the 1D marginalized parameter posteriors achieved by `Multinest`, so both samplers are used interchangeably in what follows.

A. Validation of assumptions using synthetic data

In order to verify that our results are robust to modeling assumptions and approximations, we compare the inferred values of the extension parameters (Ω_k, N_{eff}, ...) obtained by a systematically shifted, noiseless synthetic data vector. The synthetic data vector is centered precisely on the standard ΛCDM cosmology, except it is shifted with the addition of a systematic effect that is **not** included in our analysis. The goal is to ensure that we do not claim evidence for an extension to ΛCDM when the real data contains astrophysical effects more complex than those in our model. For each systematic effect, we compare the inferred set of extension parameters to the fiducial, unmodified extension parameters used to create the synthetic data (which we refer to as the "baseline" constraint). For all of these tests, for DES we use the synthetic data vectors (for the baseline case and the systematic shifts described

---

tion of CAMB, particularly when evaluating CMB lensing, sampling over many chains at full precision is impractical. We checked that this approximation has a minor effect on the shape of the posterior.

[10] https://bitbucket.org/joezuntz/cosmosis/

[11] The recommended methods for convergence testing (as well as the documentation for `emcee`) can be found in https://emcee.readthedocs.io/

below), but for the external data sets — CMB, BAO, RSD, and SN Ia — we use the actual, observed data vector.

The changes to modeling assumptions that we consider are:

1. Baryonic effects: we synthesize a noiseless data vector including a contribution to the nonlinear power spectrum caused by AGN feedback using the OWLS AGN hydrodynamical simulation [128] and following the methodology of [40].

2. Intrinsic alignments, simple case: we synthesize a noiseless data vector with the IA amplitude $A_{IA} = 0.5$ and redshift scaling $\eta_{IA} = 0.5$ using the baseline nonlinear alignment model used in Y1KP. While we explicitly marginalize over these IA parameters in our analysis, this systematic check is still useful to monitor any potential biases due to degeneracy between the cosmological parameters and (A_{IA}, η_{IA}) and the presence of non-Gaussian posteriors.

3. Intrinsic alignments, complex case: we synthesize a noiseless data vector using a subset of the Tidal Alignment and Tidal Torquing model (hereafter TATT) from [129]. This introduces a tidal torquing term to the IA spectrum that is quadratic in the tidal field. The TATT amplitudes were set to $A_1 = 0$, $A_2 = 2$ with no z dependence, as was done in [130] when validating the analysis of Y1KP.

4. Non-linear bias: we test our fiducial linear-bias assumption by synthesizing a noiseless data vector that models the density contrast of galaxies as

$$\delta_g = b_1^i \delta + \frac{1}{2} b_2^i [\delta^2 - \sigma^2] \qquad (12)$$

where δ and δ_g are the overdensities in matter and galaxy counts respectively, and and the density variance $\sigma^2 = \langle \delta^2 \rangle$ is subtracted to enforce $\langle \delta_g \rangle = 0$. While this relationship is formally defined for smoothed density fields, the results do not depend on the choice of smoothing scale since, e.g., the variance explicitly cancels with contributions to the two-point correlation. We are considering scales that are sufficiently larger than the typical region of halo formation that we neglect higher-derivative bias terms. See Ref. [131] for further discussion of nonlinear biasing. Here i refers to the lens redshift bin and where $b_1^i = \{1.45, 1.55, 1.65, 1.8, 2.0\}$ for the five bins. The b_2 values used for each lens bin were estimated from from the following relationship fit in simulations [132]: $b_2 = 0.412 - 2.143\, b_1 + 0.929\, b_1^2 + 0.008\, b_1^3$. Because the contribution from tidal bias b_{s^2} is expected to be small, we set it to zero in these validation tests.

5. Magnification: we synthesize a noiseless data vector that includes the contribution from magnification to γ_t and $w(\theta)$. These are added in Fourier space using [133].

6. Limber approximation and RSD: we synthesize a noiseless data vector that uses the exact (non-Limber) $w(\theta)$ calculation[12] and include the contribution from redshift space distortions [135].

More information about the implementation of these tests can be found in [130].

The results of these tests are shown in Fig. 2. The columns show the parameters describing ΛCDM extensions, namely w_p, w_a, Ω_k, N_{eff}, Σ_0, and μ_0. The shaded vertical region shows the marginalized 68% posterior confidence limit (CL) in each parameter for the baseline case. The horizontal error bars show how this posterior, fully marginalized over all other parameters, including the other parameter in two-parameter extensions, changes with the systematic described in the given row for the case of DES-only (blue bars) and DES+external (red bars) data. We observe that, except in the cases explained below, the marginalized posteriors are consistent with the baseline analysis in these tests[13].

Fig. 2 shows shifts in some DES-only 68% C.L. constraints relative to the input value shown by the dotted vertical lines. The most pronounced effect is in the DES-only case for modified gravity parameter μ_0 (and, to a slightly smaller extent, Σ_0 and N_{eff}), which is more than 1-σ away from its true value of zero. Upon investigating this, we found that the bias away from the input value is caused by the interplay of two effects: 1) weak constraints, with a relatively flat likelihood profile in these parameters in certain directions, combined with 2) prior-volume effect, where the large full-parameter-space volume allowed in the direction in which the parameter is a reasonably good fit ends up dominating the total integrated posterior, resulting in a 1D marginalized posterior that is skewed away from the maximum likelihood true value. For example, with the restricted range of scales that we use for the modified gravity tests, negative values of μ_0 are an acceptable (though not the best) fit and, because of the relatively large number of combinations of other parameters that result in a good likelihood for $-3 \leq \mu_0 \lesssim 0$, the 68% C.L. constraint on μ_0 ends up excluding the input best-fit value of zero (see Fig. 2). We have explicitly checked that removing the principal degeneracy with other parameters — in modified gravity tests, achieved by fixing the bias parameters b_i — removes the bias in μ_0. Nevertheless, because these tests imply that the DES-only constraint on this parameter would suffer from the aforementioned bias, we choose not to quote constraints on μ_0 from the DES-only data in the results below.

We also observe a bias in the DES+external constraint on w_a relative to the input value of zero. This is mostly driven by the fact that the best fit of the external data does not necessarily coincide with the cosmological parameter values assumed for the synthetic data vectors used to produce DES con-

_____

[12] We do not investigate the effect of the Limber approximation on the tangential shear profile γ_t, since it includes the projection from the observer to the source galaxy, and is less sensitive to the Limber approximation, below the level of the DES Y1 statistical uncertainty [134].

[13] The DES+external Ω_k column in Fig. 2 is narrow and hard to visually inspect, but we have verified that there are no biases in the curvature parameter with alternate assumptions about the systematic errors shown shown in the different rows.

straints – in fact, it is well-known that external data alone favor $w_a < 0$ [32]. Additionally, even the DES synthesized data alone mildly prefer negative w_a due to the prior-volume effect mentioned above. The resulting synthesized DES+external constraint on w_a is then biased negative at greater than 68% confidence. Because the combined analysis on the real data will not be subject to the principal cause of the w_a bias observed here, we proceed with the analysis.

There are therefore two takeaways from Fig. 2:

- First, the projected 1D inferences from DES-only measurements on μ_0 are likely to be biased principally due to the prior volume effect, so we choose not to quote constraints on this parameter in the DES-only case (but still include it in the analysis throughout). We do not attempt to correct the biases in the w_0-w_a DES+external case or inflate the parameter errors to account for it; see the discussion above.

- Second and most importantly, the different assumptions considered in Fig. 2 produce consistent results with the baseline constraint for all parameters describing ΛCDM extensions.

B. Validation of assumptions using DES data

In addition to the tests in the previous section that constrain potential biases due to our modeling assumptions and approximations on synthesized noiseless data, we implement several validation tests that modify how we analyze the actual DES data vector. In particular, we test the following assumptions:

7. Intrinsic alignments, free redshift evolution: while the fiducial analysis assumes IA to scale as a power-law in redshift (see Sec. III B), we relax that here by assuming four uncorrelated constant amplitudes per source redshift bin.

8. Conservative scales: to gauge how our results depend on the range of angular scales used, we adopt the conservative set of (basically linear) scales used in the modified gravity extension, and apply it to the other three extensions (curvature, N_{eff}, dynamical dark energy).

9. Alternate photometric redshifts: to investigate the robustness of our results to the shape of the redshift distribution of source galaxies, we adopt the distributions obtained directly from resampling the COSMOS data, as described in [39].

For each of these alternate analysis options, we investigate how the fiducial constraints on the ΛCDM extensions parameters change. These results are presented and discussed along with our main results, near the end of Sec. V.

C. Blinding

We follow the same strategy as in Y1KP, and blind the principal cosmological results to protect against human bias. We do so by shifting axes in all plots showing the cosmological parameter constraints. Where relevant, this includes simultaneously not plotting theory predictions (including simulation outputs as "theory") in those same plots. A different shift was applied to each of the DES, external data, and joint constraint contours in any figures made at the blinded stage. Moreover evidence ratios of the joint constraints were not read before unblinding. This was done to prevent confirmation bias based on the level of agreement between the DES and external constraints.

We unblinded once we ensured that there are no biases on the extension parameters due to systematics, as shown in Figs. 2 and 7, apart from those that have a known, statistical explanation (see Sec. IV A).

We have made two modifications to the analysis after the results were unblinded. First, we identified that the incorrect Planck data file (PLIK_LITE_V18_TTTEEE.CLIK) was used for our (w_0, w_a) results and reran these chains with the correct file (PLIK_LITE_V18_TT.CLIK). We verified that this modification does not lead to appreciable differences in the final constraints, though it does lead to a difference in the reported Bayesian evidence ratios for this case. Second, we adopted the GetDist code to evaluate the marginalized posteriors, as it is more suitable to handle boundary effects in the posteriors [136]. This leads to small differences in cases where the constraints are strongly informed by the prior boundaries, such as N_{eff}.

V. RESULTS

The constraints on curvature and the number of relativistic species are given in the two panels of Fig. 3. For curvature, we find

$$
\begin{aligned}
\Omega_k &= 0.16^{+0.09}_{-0.14} & \text{DES Y1} \\
&= 0.0020^{+0.0037}_{-0.0032} & \text{DES Y1 + External}
\end{aligned}
\tag{13}
$$

while for the number of relativistic species, the lower limit hits against our hard prior of $N_{\mathrm{eff}} > 3.0$ so we quote only the 68% (95%) upper limits

$$
\begin{aligned}
N_{\mathrm{eff}} &< 5.28\,(\text{—}) & \text{DES Y1} \\
&< 3.28\,(3.55) & \text{DES Y1 + External.}
\end{aligned}
\tag{14}
$$

where the dashes indicate that we do not get a meaningful upper limit from DES alone at the 95% since the constraint hits against the upper limit of our prior.

Figure 3 indicates that DES alone constrains curvature weakly, showing mild ($\sim$ 1-σ) preference for positive values of Ω_k; note also that this constraint is informed by the upper prior boundary. The DES-only constraint on N_{eff} is also relatively weak, and is fully consistent with the theoretically favored value $N_{\mathrm{eff}} = 3.046$. Moreover, the DES Y1 data do not appreciably change the existing external-data constraints on these two parameters. The addition of the DES data to external measurement does slightly suppress N_{eff}, which can
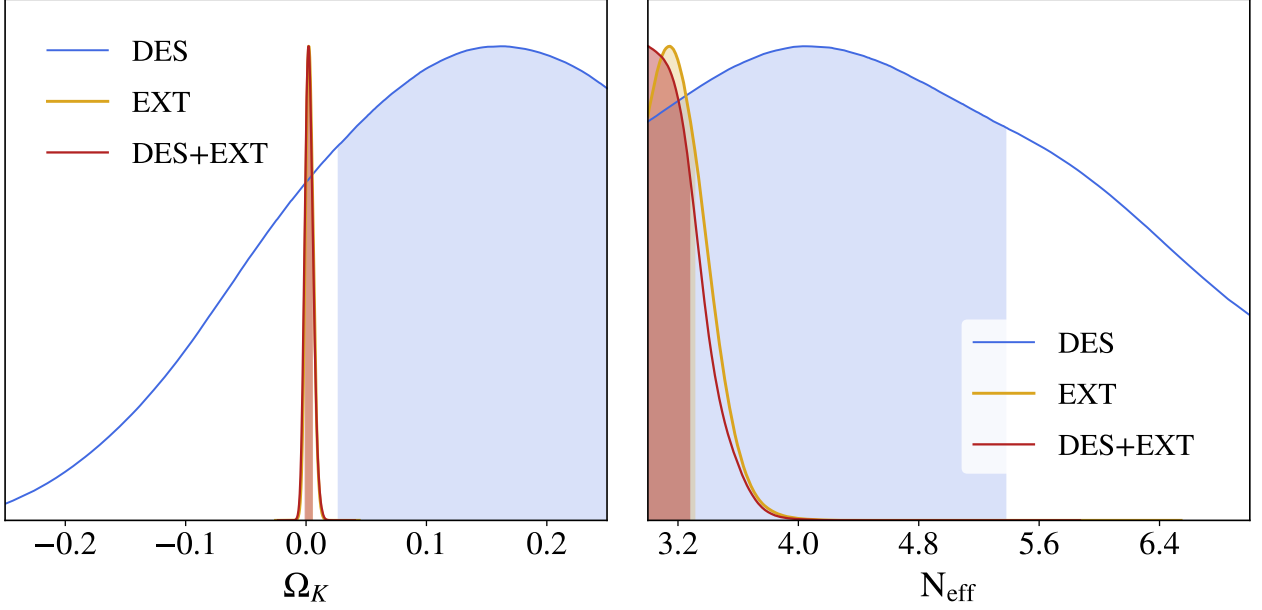
FIG. 3. Posterior constraints on the spatial curvature (left panel) and the number of relativistic species (right panel) in two of the extensions to ΛCDM considered in this paper. Blue contours show DES alone, yellow is external data alone, and red is the combination of the two. The 68% confidence region is shaded. The x-axis ranges in both panels coincide with the priors given to Ω_k and $N_{\rm eff}$, respectively. Posteriors' maxima are normalized to unity for better visibility of the DES only results.

be understood as follows. The DES data prefer a lower Ω_m than the external data, leading to a slight increase in h such that the posterior distribution in $\Omega_m h^3$ is downweighted at the high values of this parameter combination. Because $\Omega_m h^3$ is highly correlated with $N_{\rm eff}$ — they both generate out-of-phase changes in the CMB temperature power spectrum — adding DES to external data also has the consequence of slightly suppressing $N_{\rm eff}$.

We also compare the cases where the number of relativistic species is fixed at $N_{\rm eff} = 3.046$ (the standard model) and $N_{\rm eff} = 4.046$ (standard model, plus a single fully thermalized sterile neutrino). Preference for one model over the other is assessed using the evidence ratio,

$$R^{N_{\rm eff}} = \frac{P(\mathbf{d}|N_{\rm eff} = 4.046)}{P(\mathbf{d}|N_{\rm eff} = 3.046)}. \tag{15}$$

where $P(\mathbf{d}|N_{\rm eff})$ is the Bayesian evidence, given by the integral over the parameter space of the likelihood times the prior; see Eq. (5.1) in Y1KP. A ratio much greater than 1 would imply $N_{\rm eff} = 4.046$ is favored and a ratio much less than 1 would imply that $N_{\rm eff} = 3.046$ is favored. The Bayesian evidence ratios for DES alone is $R^{N_{\rm eff}} = 0.78$, indicating no statistical preference for an extra relativistic species. For the external data alone and DES plus external data, the ratios are $R^{N_{\rm eff}} = 0.0033$ and $R^{N_{\rm eff}} = 0.0049$, respectively. The combined data therefore show strong evidence to support the standard value $N_{\rm eff} = 3.046$ relative to the case with one additional relativistic species; DES does not appreciably change the result obtained using the external data alone (the apparent increase on the odds of $N_{\rm eff} = 4$ when going from external to

DES+external data is not statistically significant as the errors on R are larger than the difference between these two values.)

We now turn to dynamical dark energy. The constraints are shown in the left panel of Fig. 4. We find

$$w_0 = -0.69^{+0.30}_{-0.29}, \quad w_a = -0.57^{+0.93}_{-1.11} \quad \text{DES Y1}$$

$$= -0.95^{+0.09}_{-0.08}, \quad = -0.28^{+0.37}_{-0.48} \quad \text{DES Y1 + Ext.}$$

The DES Y1 data alone are therefore consistent with the cosmological-constant values of $(w_0, w_a) = (-1, 0)$; they do not appreciably change the constraint from external data alone.

The pivot equation-of-state (see definition in Eq. (5)) is obtained to be

$$w_p = -0.91^{+0.19}_{-0.23} \quad \text{DES Y1}$$
$$= -1.01^{+0.04}_{-0.04} \quad \text{DES Y1 + External.} \tag{16}$$

For the DES-only and DES + External cases, the pivot redshift is found to be $z_p = 0.27$ and $z_p = 0.20$, respectively. Figure 5 shows the constraints in the (w_p, w_a) plane.

Do the DES data favor the introduction of two new parameters, w_0 and w_a, to the ΛCDM model? Again, we calculate the Bayesian evidence ratio

$$R^{(w_0, w_a)} = \frac{P(\mathbf{d}|w_0, w_a)}{P(\mathbf{d}|w_0 = -1, w_a = 0)}. \tag{17}$$

For DES data alone, we find $R^{(w_0, w_a)} = 0.11$, while the DES+external data give $R^{(w_0, w_a)} = 0.006$. Therefore,
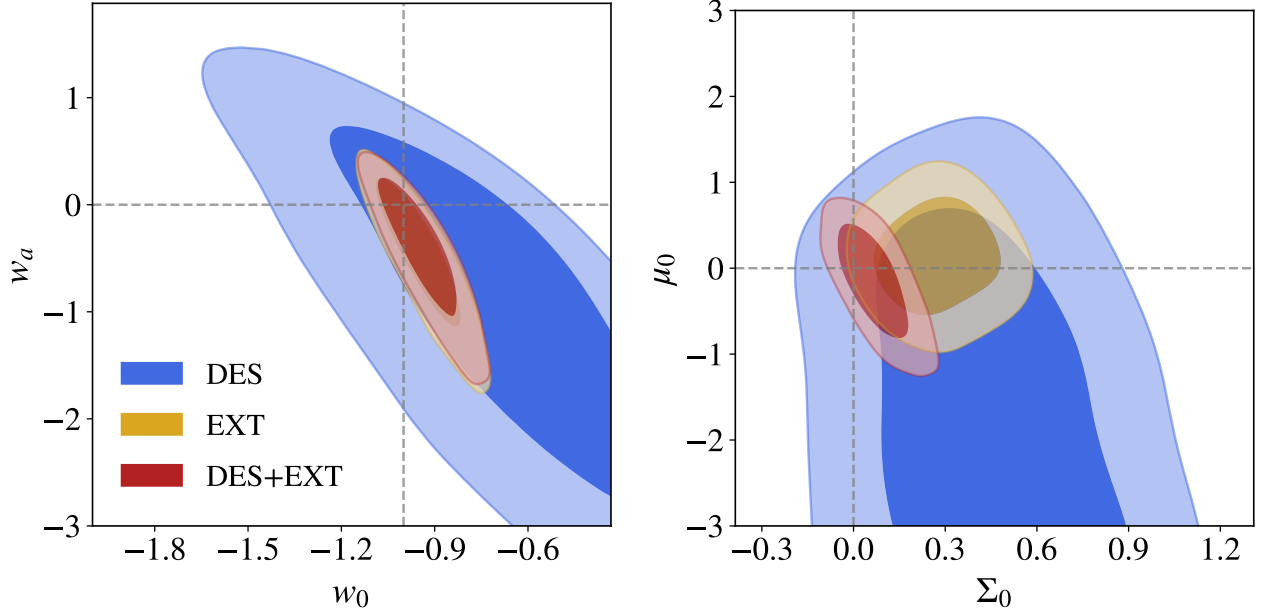
FIG. 4. Constraints on dark energy parameters (w_0, w_a) (left panel) and the modified gravity parameters (Σ_0, μ_0) (right panel). Blue contours show the 68% and 95% confidence regions from DES alone, yellow is external data alone, and red is the combination of the two. The intersection of the horizontal and vertical dashed lines shows the parameter values in the ΛCDM model (left panel) and in general relativity (right). The x-axis range in the left panel and the y-axis range in the right panel coincide with the respective priors given to w_0 and μ_0. The cause of the non-intuitive shift in the combined Σ_0 constraint (red contour) relative to separate constraints is discussed in Sec. V.

Bayesian evidence ratios strongly support ΛCDM, and do not favor introduction of the additional parameters w_0 and w_a.

Finally, we turn our attention to modified gravity, the extension for which DES carries the most weight. Recall from Sec. IV A that we have decided to quote only the constraint on the parameter Σ_0 in the DES-only case. The constraint, shown in the right panel of Fig. 4, is

$$\Sigma_0 = 0.43^{+0.28}_{-0.29} \qquad \text{DES Y1}$$

$$\Sigma_0 = 0.06^{+0.08}_{-0.07}, \quad \mu_0 = -0.11^{+0.42}_{-0.46} \quad \text{DES Y1 + Ext,}$$
$$(18)$$

the latter of which can be compared to the external-only constraint, which is $\Sigma_0 = 0.28^{+0.13}_{-0.14}$. Thus the addition of DES data improves the constraints on Σ_0 by almost a factor of two.

Besides the tighter constraint, DES also pushes Σ_0 closer to its ΛCDM value of zero. An interesting manifestation of the multi-dimensionality of the parameter space is that the DES+external value is lower than either DES or external alone. This arises because DES favors a lower amplitude of mass fluctuations than that favored by the external data, due to the lower amplitude of the lensing signal observed by the DES. Because the lensing amplitude is proportional to the product $\Sigma_0 S_8$, these two parameters are highly anti-correlated in DES, and the lensing amplitude suppression can be accommodated by decreasing either of them. Since external data constrain mostly S_8 and constrain it to be high, the DES lensing amplitude is accommodated by shifting Σ_0 down.

The constraints on the extensions parameters are summa-

rized in Table III. The last column in the Table shows the improvement in the goodness-of-fit between the corresponding best-fit extension and the best-fit ΛCDM model, and indicates that none of the extensions are strongly preferred relative to ΛCDM.

In Fig. 6, we show the constraints in the Ω_m-S_8 plane for the extended models (solid contours); for comparison, we also show the ΛCDM model constraints for DES data alone (dashed contours which are the same in all panels). The top right corner of each panel shows which extension the plot is referring to. For Ω_k, N_{eff} and w_0-w_a extensions, we see that the Ω_m-S_8 contour from DES alone is only modestly increased by marginalization over the additional nuisance parameter(s). The exception is the modified-gravity case, where the Ω_m-S_8 contour from DES alone is significantly larger and also pushed to smaller values of S_8 because of the amplitude degeneracy between Σ_0 and S_8.

Furthermore, Fig. 7 shows the results of the systematic tests on the analysis assumptions outlined in Sec. IV B. The top row shows our fiducial constraints on the extensions parameters presented earlier in this Section, relative to the corresponding marginalized best-fit value in the same fiducial analysis. The next three rows show these constraints (still relative to the corresponding best-fit value in the fiducial analysis): assuming alternative treatment of intrinsic alignments; the use of conservative scales (except in the modified-gravity extension which assumes them by default); and adopting alternative photometric redshifts. The results show no significant biases in the results on the extensions parameters, providing further support that our modeling is robust with respect to our mod-

TABLE III. Constraints on the parameters describing the extensions of the ΛCDM model that we study in this paper. All errors are 68% confidence intervals, except for N_{eff} where we show the 68% upper bound. We do not quote the DES-only constraint on μ_0, as discussed in Sec. IV A. The last column shows the improvement in the goodness-of-fit, $\Delta\chi^2$, between the corresponding best-fit extension and the best-fit ΛCDM. Note that the sampling error in the $\Delta\chi^2$ values is ~ 0.5; hence, the two positive values in the last column (and many of the negative ones) should be treated as consistent with zero.

Curvature	DES Y1	External	DES Y1 + External	$[(\Delta\chi^2)_{\text{DES}}, (\Delta\chi^2)_{\text{Ext}}, (\Delta\chi^2)_{\text{DES+Ext}}]$
Ω_k	$0.16^{+0.09}_{-0.14}$	$0.0023^{+0.0035}_{-0.0030}$	$0.0020^{+0.0037}_{-0.0032}$	$[-0.9, -0.2, -0.1]$
Number Rel. Species	DES Y1	External	DES Y1 + External	$[(\Delta\chi^2)_{\text{DES}}, (\Delta\chi^2)_{\text{Ext}}, (\Delta\chi^2)_{\text{DES+Ext}}]$
N_{eff}	< 5.38	< 3.32	< 3.28	$[0.2, 0.4, -0.7]$
Dynamical dark energy	DES Y1	External	DES Y1 + External	$[(\Delta\chi^2)_{\text{DES}}, (\Delta\chi^2)_{\text{Ext}}, (\Delta\chi^2)_{\text{DES+Ext}}]$
w_0	$-0.69^{+0.30}_{-0.29}$	$-0.96^{+0.10}_{-0.08}$	$-0.95^{+0.09}_{-0.08}$	
w_a	$-0.57^{+0.93}_{-1.11}$	$-0.31^{+0.38}_{-0.52}$	$-0.28^{+0.37}_{-0.48}$	$[-1.9, -0.0, -0.1]$
w_p	$-0.91^{+0.19}_{-0.23}$	$-1.02^{+0.04}_{-0.04}$	$-1.01^{+0.04}_{-0.04}$	
Modified Gravity	DES Y1	External	DES Y1 + External	$[(\Delta\chi^2)_{\text{DES}}, (\Delta\chi^2)_{\text{Ext}}, (\Delta\chi^2)_{\text{DES+Ext}}]$
Σ_0	$0.43^{+0.28}_{-0.29}$	$0.26^{+0.14}_{-0.13}$	$0.06^{+0.08}_{-0.07}$	$[-0.2, -3.4, -0.4]$
μ_0	—	$0.16^{+0.43}_{-0.47}$	$-0.11^{+0.42}_{-0.46}$	
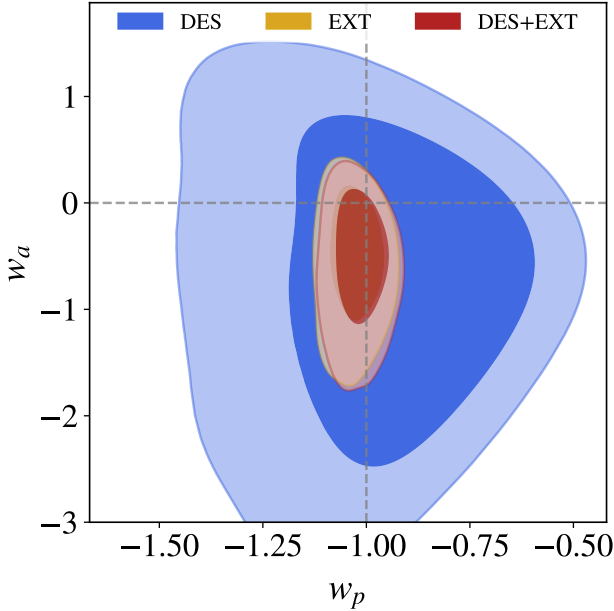
FIG. 5. Constraints on the pivot value of the dark energy equation-of-state w_p and the variation with scale factor w_a Blue contours show DES alone, yellow is external data alone, and red is the combination of the two. The intersection of the horizontal and vertical dashed lines shows the parameter values in the ΛCDM model.

eling of intrinsic alignments, angular scales used, and photometric redshifts.

We now compare our extended-model cosmological con-straints to those obtained using KiDS-450 [28] shear measurements, and to the Planck 2018 (P18) CMB measurements [32]. KiDS analysis is similar to ours in that they use their own shear measurements combined with external data; one difference is that we use the full 3×2 data vector which, in addition to shear, also includes galaxy clustering and galaxy-galaxy lensing[14]. Planck, on the other hand, uses the DES Y1 shear measurements as an external weak lensing data set, combining it with their CMB information. It is important to note that both KiDS and Planck fix the neutrino mass to $\sum m_\nu = 0.06$eV in their baseline ΛCDM model, while we vary the neutrino mass as part of the fiducial model. Therefore, our cosmological constraints are expected to be weaker, but more robust with respect to the neutrino mass, than they would be with the same assumptions as KiDS and P18.

Comparison with KiDS-450 will be necessarily qualitative, given that they do not quote the numerical values of their constraints on the cosmological parameters. KiDS do not consider N_{eff} as one of their extensions, but they do study curvature, finding some preference for a negative Ω_k (see their Fig. 8b), which is in the opposite direction of our mild preference for positive Ω_k. Their w_0-w_a constraint, like ours, is broadly consistent with the ΛCDM scenario with values of -1 and zero, respectively. Their phenomenological

---

[14] In their extended work [48], KiDS combine their own shear measurements with galaxy clustering and RSD information from 2-degree Field Lensing Survey (2dFLenS) and the Baryon Oscillation Spectroscopic Survey (BOSS), effectively using a (3×2)-type data vector. Here we choose to compare our DES-only results to KiDS-only results presented in Ref. [28]. We thank Shahab Joudaki for pointing this out.
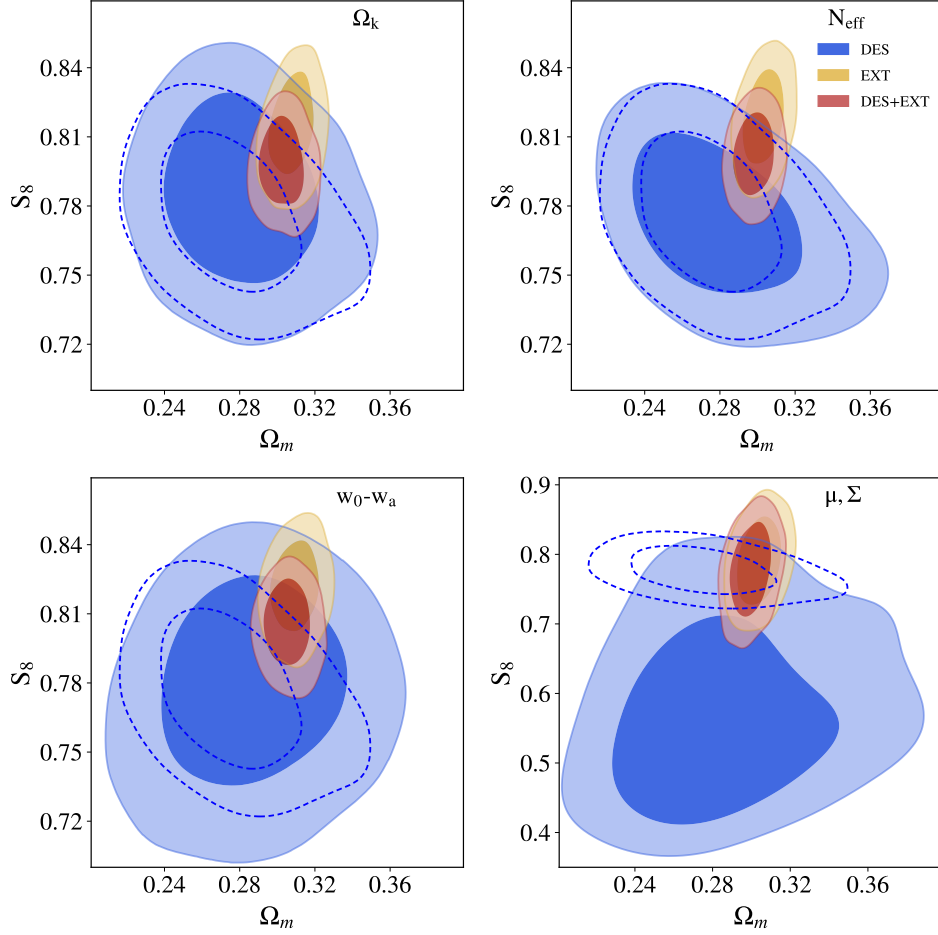
FIG. 6. Comparison of constraints on the matter density Ω_m and S_8 to the ΛCDM case. The panels illustrate how the Ω_m-S_8 constraints broaden and shift as we allow to vary: curvature (*top left*), number of relativistic species (*top right*), equation-of-state parameters w_0 and w_a (*bottom left*), and modified gravity parameters Σ_0 and μ_0 (*bottom right*). In each case, the shaded contours denote DES (blue), external (yellow), and DES+external (red) constraints. For comparison, in the DES-only case we also show the constraints in the ΛCDM model with dashed contours, which are the same in each panel.

tests of gravity assumed the (Q, Σ) parameterization, where $Q_{\mathrm{KiDS}} = 1 + 2\Sigma_{\mathrm{DES}} - \mu_{\mathrm{DES}}$ and $\Sigma_{\mathrm{KiDS}} = 1 + \Sigma_{\mathrm{DES}}$, so that general relativity corresponds to their $(Q, \Sigma) = (1, 1)$. They described each of their functions Q and Σ by piecewise constant values across two bins in scale and two in redshift, so that their analysis included eight modified-gravity parameters as opposed to two in the present paper. Comparing DES and KiDS modified-gravity results is therefore not straightforward but we can study the main trends. The parameters (Q_2, Σ_2) corresponding to the modified gravity parameters in the low redshift bin and small-scale (high-k) bin are the best constrained by KiDS and are shown in figure 13 of [28]. Much like we see in our own results, KiDS measurements help constrain Σ as it is directly linked to the lensing potential. Interestingly, KiDS results are consistent with very positive values of Q_2 (although they are also consistent with the standard value $Q_2 = 1$), which corresponds to DES's preference for a positive Σ_0 and negative μ_0 shown in the right panel of Fig. 4. On the whole, the different temporal and spatial

parametrizations of modified gravity functions in KiDS and DES Y1, along with other differences in the two analyses, make detailed comparisons impossible, but the two surveys' constraints on modified gravity seem in broad agreement.

For comparison with Planck we only consider the modified-gravity case, as this is the ΛCDM extension where DES Y1 information appreciably improves the constraints obtained from Planck and other external data. P18 constraints on modified gravity [32] employ the base parameters μ and η, with $\mu_{\mathrm{P18}} = 1 + \mu_{\mathrm{DES}}$ being defined to have the redshift variation same as ours in Eq. (10); they also quote constraints on $\Sigma_{\mathrm{P18}} = 1 + \Sigma_{\mathrm{DES}}$, whose redshift dependence however does not coincide with ours. Planck considers a similar set of other data as we do: their SN and RSD datasets are identical to ours; they use a more extensive selection of BAO data, but their DES information includes only the weak lensing (shear) information and not the full 3×2 data vector as in the present paper. Therefore, a somewhat direct although not exact comparison of the combined constraints between DES Y1 and P18

DES Y1

Fiducial Analysis

Free IA *z*-evolution

Conservative scale cuts

COSMOS photo-*z*s
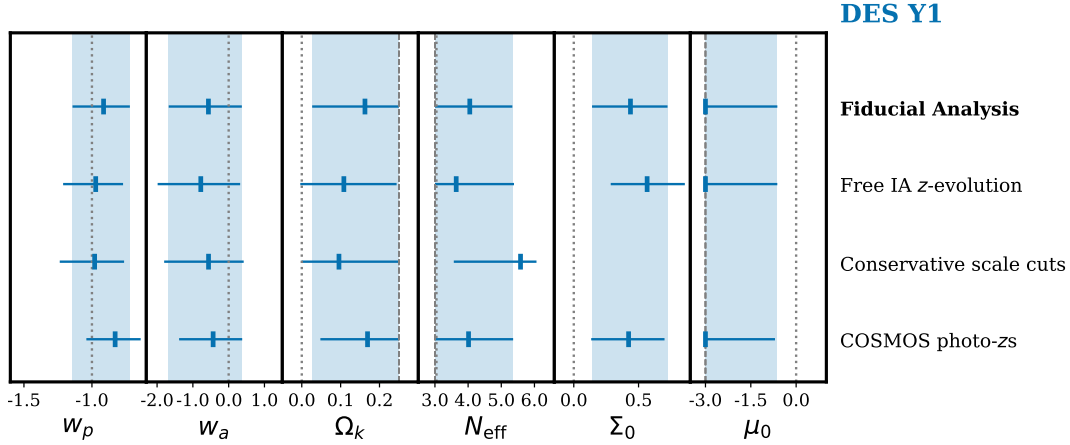
FIG. 7. Impact of changes in modeling assumptions to the inferred cosmology, using actual (and not synthesized as in Fig. 2) DES data. Each column shows one of the cosmological parameters describing ΛCDM extensions. The horizontal error bars show the constraints for each individual change in the analysis, listed to the right of the Figure. The vertical shaded band coincides with the horizontal error bars in the fiducial-analysis case. The modified-gravity analysis assumes conservative scale cuts as a default, so the corresponding test is left blank in the table.

is possible. We refer to Table 7 of [32] where P18 report constraints from the combination of Planck and external data, the latter of which includes DES Y1 shear. The central values of Σ_0 and μ_0 in our DES+external analysis are very close to the corresponding values in P18. Our DES+external errors on Σ_0 (μ_0) are about 30% (80%) weaker that those in P18, which is probably chiefly due to our marginalization over neutrino mass, and possibly also to the aforementioned differences in the selected data sets. On the whole, the DES and P18 constraints that combine all data are consistent both mutually and with predictions of general relativity.

The new information that the DES Y1 data contribute to the overall constraints on modified gravity that we presented in this paper illustrates that near-future DES data should provide sharp tests of the modified-gravity paradigm.

VI. CONCLUSIONS

The results in this paper extend the work done in the Y1KP [35] by analyzing the models beyond flat ΛCDM and wCDM. In Y1KP, we found good agreement with the standard cosmological-constant dominated universe, and produced constraints on the matter density and amplitude of mass fluctuations comparable to those from the Planck satellite. We now extend that work into four new directions, allowing for: 1) nonzero curvature Ω_k; 2) number of relativistic species N_{eff} different from the standard value of 3.046; 3) time-varying equation-of-state of dark energy described by the parameters w_0 and w_a (alternatively, the values at the pivot redshift w_p and w_a); and 4) modified gravity described by the parameters Σ_0, μ_0 that modify the metric potentials.

For the first three of these four extensions, we find that the DES Y1 data alone are consistent with values of zero curvature, three relativistic species, and dark energy parameters corresponding to the cosmological constant model. We also find

that DES Y1 data do not significantly improve the existing constraints which combine the Planck 2015 temperature and polarization measurements, BAO measurements from SDSS and BOSS, RSD measurements from BOSS, and type Ia supernova measurements from the Pantheon compilation. When DES Y1 information is combined with that from the external data, the constraints on curvature are $\Omega_k = 0.0020^{+0.0037}_{-0.0032}$, while that on the dark-energy equation of state pivot value and its variation are $w_p = -1.01^{+0.04}_{-0.04}$ and $w_a = -0.28^{+0.37}_{-0.48}$, respectively. The upper bound on the number of relativistic species is $N_{\text{eff}} < 3.28(3.55)$ at the 68% (95%) confidence level from the combination of DES and external data.

DES Y1 alone provides a stronger constraint on the fourth extension of ΛCDM that we consider – modified gravity – giving $\Sigma_0 = 0.43^{+0.28}_{-0.29}$. The apparent DES-alone preference for positive Σ_0 is consistent with parameter volume effects discussed in Sec. IV A. When combining DES with external data, the Σ_0 constraint is shifted downwards with respect to the external-only constraint, which can be explained by the fact that DES data prefer a lower lensing amplitude than that predicted by external data in ΛCDM. Combining DES Y1 with the external data gives $\Sigma_0 = 0.06^{+0.08}_{-0.07}$ and $\mu_0 = -0.11^{+0.42}_{-0.46}$, both of which are fully consistent with the ΛCDM values $(\Sigma_0, \mu_0) = (0, 0)$.

We applied a suite of validation and null tests both to our analysis and to our theory modeling; the results of these tests are shown in Figs. 2 and 7. In nontrivial model spaces such as modified gravity, we compared the results obtained by two independently developed parameter inference pipelines, `CosmoLike` and `CosmoSIS`, and also compared the constraints used obtained using two different samplers, `emcee` and `multinest`. We modeled any remaining systematics with 20 nuisance parameters, marginalizing over them to get the constraints on cosmological parameters. Finally, in all cases we applied the parameter-level blinding procedure, and did not look at the final cosmological constraints until after

unblinding.

The results in this paper also serve to develop the tools necessary to take advantage of future constraints on these cosmological models by DES. In particular, the forthcoming analysis of the DES Y3 data, which will contain information from three times the area of Y1, should provide very interesting constraints on extensions of the minimal cosmological model including dark energy and modified gravity.

[1] F. Zwicky, Helv. Phys. Acta **6**, 110 (1933), [Gen. Rel. Grav.41,207(2009)].

[2] A. G. Riess *et al.* (Supernova Search Team), Astron. J. **116**, 1009 (1998), arXiv:astro-ph/9805201 [astro-ph].

[3] S. Perlmutter *et al.* (Supernova Cosmology Project), Astrophys. J. **517**, 565 (1999), arXiv:astro-ph/9812133 [astro-ph].

[4] J. Frieman, M. Turner, and D. Huterer, Ann. Rev. Astron. Astrophys. **46**, 385 (2008), arXiv:0803.0982 [astro-ph].

[5] D. H. Weinberg, M. J. Mortonson, D. J. Eisenstein, C. Hirata, A. G. Riess, and E. Rozo, Phys. Rept. **530**, 87 (2013),

arXiv:1201.2434 [astro-ph.CO].

[6] D. Huterer and D. L. Shafer, Rept. Prog. Phys. **81**, 016901 (2018), arXiv:1709.01091 [astro-ph.CO].

[7] W. Hu and S. Dodelson, Ann. Rev. Astron. Astrophys. **40**, 171 (2002), arXiv:astro-ph/0110414 [astro-ph].

[8] H. Hoekstra and B. Jain, Ann. Rev. Nucl. Part. Sci. **58**, 99 (2008), arXiv:0805.0139 [astro-ph].

[9] S. W. Allen, A. E. Evrard, and A. B. Mantz, Ann. Rev. Astron. Astrophys. **49**, 409 (2011), arXiv:1103.4829 [astro-ph.CO].

[10] S. Weinberg, Rev. Mod. Phys. **61**, 1 (1989).

[11] J. Martin, Comptes Rendus Physique **13**, 566 (2012), arXiv:1205.3365 [astro-ph.CO].

[12] A. Joyce, B. Jain, J. Khoury, and M. Trodden, Phys. Rept. **568**, 1 (2015), arXiv:1407.0059 [astro-ph.CO].

[13] P. Bull *et al.*, Phys. Dark Univ. **12**, 56 (2016), arXiv:1512.05356 [astro-ph.CO].

[14] M. Ishak, Living Rev. Rel. **22**, 1 (2019), arXiv:1806.10122 [astro-ph.CO].

[15] B. Jain and P. Zhang, Phys. Rev. **D78**, 063503 (2008), arXiv:0709.2375 [astro-ph].

[16] P. Zhang, Phys. Rev. **D73**, 123504 (2006), arXiv:astro-ph/0511218 [astro-ph].

[17] R. Caldwell, A. Cooray, and A. Melchiorri, Phys. Rev. **D76**, 023507 (2007), arXiv:astro-ph/0703375 [ASTRO-PH].

[18] J. Guzik, B. Jain, and M. Takada, Phys. Rev. **D81**, 023503 (2010), arXiv:0906.2221 [astro-ph.CO].

[19] R. Bean and M. Tangmatitham, Phys. Rev. **D81**, 083534 (2010), arXiv:1002.4197 [astro-ph.CO].

[20] G.-B. Zhao, T. Giannantonio, L. Pogosian, A. Silvestri, D. J. Bacon, K. Koyama, R. C. Nichol, and Y.-S. Song, Phys. Rev. **D81**, 103510 (2010), arXiv:1003.0001 [astro-ph.CO].

[21] R. Reyes, R. Mandelbaum, U. Seljak, T. Baldauf, J. E. Gunn, L. Lombriser, and R. E. Smith, Nature **464**, 256 (2010), arXiv:1003.2185 [astro-ph.CO].

[22] S. F. Daniel, E. V. Linder, T. L. Smith, R. R. Caldwell, A. Cooray, A. Leauthaud, and L. Lombriser, Phys. Rev. **D81**, 123508 (2010), arXiv:1002.1962 [astro-ph.CO].

[23] G.-B. Zhao, R. G. Crittenden, L. Pogosian, and X. Zhang, Phys. Rev. Lett. **109**, 171301 (2012), arXiv:1207.3804 [astro-ph.CO].

[24] S. F. Daniel and E. V. Linder, JCAP **1302**, 007 (2013), arXiv:1212.0009 [astro-ph.CO].

[25] P. A. R. Ade *et al.* (Planck), Astron. Astrophys. **594**, A14 (2016), arXiv:1502.01590 [astro-ph.CO].

[26] A. Hojjati, A. Plahn, A. Zucca, L. Pogosian, P. Brax, A.-C. Davis, and G.-B. Zhao, Phys. Rev. **D93**, 043531 (2016), arXiv:1511.05962 [astro-ph.CO].

[27] V. Salvatelli, F. Piazza, and C. Marinoni, JCAP **1609**, 027 (2016), arXiv:1602.08283 [astro-ph.CO].

[28] S. Joudaki *et al.*, Mon. Not. Roy. Astron. Soc. **471**, 1259 (2017), arXiv:1610.04606 [astro-ph.CO].

[29] E.-M. Mueller, W. Percival, E. Linder, S. Alam, G.-B. Zhao, A. G. Snchez, F. Beutler, and J. Brinkmann, Mon. Not. Roy. Astron. Soc. **475**, 2122 (2018), arXiv:1612.00812 [astro-ph.CO].

[30] G.-B. Zhao *et al.*, Nat. Astron. **1**, 627 (2017), arXiv:1701.08165 [astro-ph.CO].

[31] A. Amon *et al.*, Mon. Not. Roy. Astron. Soc. **479**, 3422 (2018), arXiv:1711.10999 [astro-ph.CO].

[32] N. Aghanim *et al.* (Planck), (2018), arXiv:1807.06209 [astro-ph.CO].

[33] T. Abbott *et al.* (DES), (2005), arXiv:astro-ph/0510346 [astro-ph].

[34] B. Flaugher *et al.*, The Astronomical Journal **150**, 150 (2015), arXiv:1504.02900 [astro-ph.IM].

[35] T. M. C. Abbott *et al.* (DES), Phys. Rev. **D98**, 043526 (2018), arXiv:1708.01530 [astro-ph.CO].

[36] E. Krause *et al.* (DES), Submitted to: Phys. Rev. D (2017), arXiv:1706.09359 [astro-ph.CO].

[37] N. MacCrann *et al.* (DES), Mon. Not. Roy. Astron. Soc. **480**, 4614 (2018), arXiv:1803.09795 [astro-ph.CO].

[38] J. Zuntz *et al.* (DES), Mon. Not. Roy. Astron. Soc. **481**, 1149 (2018), arXiv:1708.01533 [astro-ph.CO].

[39] B. Hoyle *et al.* (DES), Mon. Not. Roy. Astron. Soc. **478**, 592 (2018), arXiv:1708.01532 [astro-ph.CO].

[40] M. A. Troxel *et al.* (DES), Phys. Rev. **D98**, 043528 (2018), arXiv:1708.01538 [astro-ph.CO].

[41] J. Prat *et al.* (DES), Phys. Rev. **D98**, 042005 (2018), arXiv:1708.01537 [astro-ph.CO].

[42] J. Elvin-Poole *et al.* (DES), Phys. Rev. **D98**, 042006 (2018), arXiv:1708.01536 [astro-ph.CO].

[43] P. A. R. Ade *et al.* (Planck), Astron. Astrophys. **594**, A13 (2016), arXiv:1502.01589 [astro-ph.CO].

[44] F. Beutler, C. Blake, M. Colless, D. H. Jones, L. Staveley-Smith, L. Campbell, Q. Parker, W. Saunders, and F. Watson, Mon. Not. Roy. Astron. Soc. **416**, 3017 (2011), arXiv:1106.3366 [astro-ph.CO].

[45] A. J. Ross, L. Samushia, C. Howlett, W. J. Percival, A. Burden, and M. Manera, Mon. Not. Roy. Astron. Soc. **449**, 835 (2015), arXiv:1409.3242 [astro-ph.CO].

[46] S. Alam *et al.* (BOSS), Mon. Not. Roy. Astron. Soc. **470**, 2617 (2017), arXiv:1607.03155 [astro-ph.CO].

[47] M. Betoule *et al.* (SDSS), Astron. Astrophys. **568**, A22 (2014), arXiv:1401.4064 [astro-ph.CO].

[48] S. Joudaki *et al.*, Mon. Not. Roy. Astron. Soc. **474**, 4894 (2018), arXiv:1707.06627 [astro-ph.CO].

[49] D. M. Scolnic *et al.*, Astrophys. J. **859**, 101 (2018), arXiv:1710.00845 [astro-ph.CO].

[50] S. Desai *et al.* (2012) p. 83, arXiv:1204.1210 [astro-ph.CO].

[51] I. Sevilla *et al.* (DES Collaboration) (2011) arXiv:1109.6741 [astro-ph.IM].

[52] J. J. Mohr *et al.* (DES Collaboration) (2008) p. 0, arXiv:0807.2515.

[53] E. Morganson *et al.* (DES), Publ. Astron. Soc. Pac. **130**, 074501 (2018), arXiv:1801.03177 [astro-ph.IM].

[54] A. Drlica-Wagner *et al.* (DES), Astrophys. J. Suppl. **235**, 33 (2018), arXiv:1708.01531 [astro-ph.CO].

[55] E. Rozo *et al.* (DES), Mon. Not. Roy. Astron. Soc. **461**, 1431 (2016), arXiv:1507.05460 [astro-ph.IM].

[56] R. Cawthon *et al.* (DES), Mon. Not. Roy. Astron. Soc. **481**, 2427 (2018), arXiv:1712.07298 [astro-ph.CO].

[57] E. Huff and R. Mandelbaum, (2017), arXiv:1702.02600 [astro-ph.CO].

[58] E. S. Sheldon and E. M. Huff, Astrophys. J. **841**, 24 (2017), arXiv:1702.02601 [astro-ph.CO].

[59] D. Coe, N. Benitez, S. F. Sanchez, M. Jee, R. Bouwens, and H. Ford, Astron. J. **132**, 926 (2006), arXiv:astro-ph/0605262 [astro-ph].

[60] C. Davis *et al.* (DES), Submitted to: Mon. Not. Roy. Astron. Soc. (2017), arXiv:1710.02517 [astro-ph.CO].

[61] M. Gatti *et al.* (DES), Mon. Not. Roy. Astron. Soc. **477**, 1664 (2018), arXiv:1709.00992 [astro-ph.CO].

[62] M. Jarvis, G. Bernstein, and B. Jain, Mon. Not. Roy. Astron. Soc. **352**, 338 (2004), arXiv:astro-ph/0307393 [astro-ph].

[63] E. Krause and T. Eifler, Mon. Not. Roy. Astron. Soc. **470**, 2100 (2017), arXiv:1601.05779 [astro-ph.CO].

[64] A. Cooray and R. K. Sheth, Phys. Rept. **372**, 1 (2002), arXiv:astro-ph/0206508 [astro-ph].

[65] M. A. Troxel *et al.* (DES), Mon. Not. Roy. Astron. Soc. **479**, 4998 (2018), arXiv:1804.10663 [astro-ph.CO].

[66] J. Zhang, L. Hui, and A. Stebbins, Astrophys. J. **635**, 806 (2005), arXiv:astro-ph/0312348 [astro-ph].

[67] S. Wang, L. Hui, M. May, and Z. Haiman, Phys. Rev. **D76**, 063503 (2007), arXiv:0705.0165 [astro-ph].

[68] A. Abate and O. Lahav, Mon. Not. Roy. Astron. Soc. **389**, 47 (2008), arXiv:0805.3160 [astro-ph].

[69] E. J. Ruiz and D. Huterer, Phys. Rev. **D91**, 063009 (2015), arXiv:1410.5832 [astro-ph.CO].

[70] J. L. Bernal, L. Verde, and A. J. Cuesta, JCAP **1602**, 059 (2016), arXiv:1511.03049 [astro-ph.CO].

[71] N. Aghanim *et al.* (Planck), Astron. Astrophys. **594**, A11 (2016), arXiv:1507.02704 [astro-ph.CO].

[72] P. A. R. Ade *et al.* (Planck), Astron. Astrophys. **594**, A15 (2016), arXiv:1502.01591 [astro-ph.CO].

[73] D. Scolnic *et al.*, Astrophys. J. **815**, 117 (2015), arXiv:1508.05361 [astro-ph.IM].

[74] A. Lewis, A. Challinor, and A. Lasenby, Astrophys. J. **538**, 473 (2000), arXiv:astro-ph/9911177 [astro-ph].

[75] J. Lesgourgues, ArXiv e-prints (2011), arXiv:1104.2932 [astro-ph.IM].

[76] R. E. Smith, J. A. Peacock, A. Jenkins, S. D. M. White, C. S. Frenk, F. R. Pearce, P. A. Thomas, G. Efstathiou, and H. M. P. Couchmann (VIRGO Consortium), Mon. Not. Roy. Astron. Soc. **341**, 1311 (2003), arXiv:astro-ph/0207664 [astro-ph].

[77] R. Takahashi, M. Sato, T. Nishimichi, A. Taruya, and M. Oguri, Astrophys. J. **761**, 152 (2012), arXiv:1208.2701 [astro-ph.CO].

[78] S. Bird, M. Viel, and M. G. Haehnelt, Mon. Not. Roy. Astron. Soc. **420**, 2551 (2012), arXiv:1109.4416 [astro-ph.CO].

[79] C. D. Leonard, P. Bull, and R. Allison, Phys. Rev. **D94**, 023502 (2016), arXiv:1604.01410 [astro-ph.CO].

[80] G. Aslanyan and R. Easther, Phys. Rev. **D91**, 123523 (2015), arXiv:1504.03682 [astro-ph.CO].

[81] M. C. Johnson and W. Lin, JCAP **1603**, 051 (2016), arXiv:1508.03786 [astro-ph.CO].

[82] D. A. Dicus, E. W. Kolb, A. M. Gleeson, E. C. G. Sudarshan, V. L. Teplitz, and M. S. Turner, Phys. Rev. **D26**, 2694 (1982).

[83] S. Dodelson and M. S. Turner, Phys. Rev. **D46**, 3372 (1992).

[84] G. Mangano, G. Miele, S. Pastor, T. Pinto, O. Pisanti, and P. D. Serpico, Nucl. Phys. **B729**, 221 (2005), arXiv:hep-ph/0506164 [hep-ph].

[85] M. Gell-Mann, P. Ramond, and R. Slansky, Conf. Proc. **C790927**, 315 (1979), arXiv:1306.4669 [hep-th].

[86] S. Dodelson and L. M. Widrow, Phys. Rev. Lett. **72**, 17 (1994), arXiv:hep-ph/9303287 [hep-ph].

[87] A. Aguilar-Arevalo *et al.* (LSND), Phys. Rev. **D64**, 112007 (2001), arXiv:hep-ex/0104049 [hep-ex].

[88] A. A. Aguilar-Arevalo *et al.* (MiniBooNE), Phys. Rev. Lett. **121**, 221801 (2018), arXiv:1805.12028 [hep-ex].

[89] R. Essig *et al.* (2013) arXiv:1311.0029 [hep-ph].

[90] O. Pisanti, A. Cirillo, S. Esposito, F. Iocco, G. Mangano, G. Miele, and P. D. Serpico, Comput. Phys. Commun. **178**, 956 (2008), arXiv:0705.0290 [astro-ph].

[91] E. V. Linder, Phys. Rev. Lett. **90**, 091301 (2003), astro-ph/0208512.

[92] M. J. Francis, G. F. Lewis, and E. V. Linder, Mon. Not. Roy. Astron. Soc. **380**, 1079 (2007), arXiv:0704.0312 [astro-ph].

[93] L. Casarini, S. A. Bonometto, E. Tessarotto, and P. S. Corasaniti, JCAP **1608**, 008 (2016), arXiv:1601.07230 [astro-ph.CO].

[94] E. Lawrence, K. Heitmann, J. Kwan, A. Upadhye, D. Bingham, S. Habib, D. Higdon, A. Pope, H. Finkel, and N. Frontiere, Astrophys. J. **847**, 50 (2017), arXiv:1705.03388 [astro-ph.CO].

[95] S. M. Carroll, M. Hoffman, and M. Trodden, Phys. Rev. **D68**, 023509 (2003), arXiv:astro-ph/0301273 [astro-ph].

[96] F. Simpson *et al.*, Mon. Not. Roy. Astron. Soc. **429**, 2249 (2013), arXiv:1212.3339 [astro-ph.CO].

[97] A. Ferté, D. Kirk, A. R. Liddle, and J. Zuntz, Phys. Rev. **D99**, 083512 (2019), arXiv:1712.01846 [astro-ph.CO].

[98] L. Lombriser and A. Taylor, JCAP **1603**, 031 (2016), arXiv:1509.08458 [astro-ph.CO].

[99] L. Lombriser and N. A. Lima, Phys. Lett. **B765**, 382 (2017), arXiv:1602.07670 [astro-ph.CO].

[100] J. Sakstein and B. Jain, Phys. Rev. Lett. **119**, 251303 (2017), arXiv:1710.05893 [astro-ph.CO].

[101] J. M. Ezquiaga and M. Zumalacrregui, Phys. Rev. Lett. **119**, 251304 (2017), arXiv:1710.05901 [astro-ph.CO].

[102] S. Boran, S. Desai, E. O. Kahya, and R. P. Woodard, Phys. Rev. **D97**, 041501 (2018), arXiv:1710.06168 [astro-ph.HE].

[103] T. Baker, E. Bellini, P. G. Ferreira, M. Lagos, J. Noller, and I. Sawicki, Phys. Rev. Lett. **119**, 251301 (2017), arXiv:1710.06394 [astro-ph.CO].

[104] R. Kase and S. Tsujikawa, Phys. Rev. **D97**, 103501 (2018), arXiv:1802.02728 [gr-qc].

[105] B. Abbott *et al.* (Virgo, LIGO Scientific), Phys. Rev. Lett. **119**, 161101 (2017), arXiv:1710.05832 [gr-qc].

[106] A. Silvestri, L. Pogosian, and R. V. Buniy, Phys. Rev. **D87**, 104015 (2013), arXiv:1302.1193 [astro-ph.CO].

[107] T. Baker, P. G. Ferreira, and C. Skordis, Phys. Rev. **D87**, 024015 (2013), arXiv:1209.2117 [astro-ph.CO].

[108] P. Creminelli, G. D'Amico, J. Norena, and F. Vernizzi, JCAP **0902**, 018 (2009), arXiv:0811.0827 [astro-ph].

[109] T. Baker, P. G. Ferreira, C. Skordis, and J. Zuntz, Phys. Rev. **D84**, 124018 (2011), arXiv:1107.0491 [astro-ph.CO].

[110] R. A. Battye and J. A. Pearson, JCAP **1207**, 019 (2012), arXiv:1203.0398 [hep-th].

[111] J. Gleyzes, D. Langlois, F. Piazza, and F. Vernizzi, JCAP **1308**, 025 (2013), arXiv:1304.4840 [hep-th].

[112] J. Gleyzes, D. Langlois, F. Piazza, and F. Vernizzi, JCAP **1502**, 018 (2015), arXiv:1408.1952 [astro-ph.CO].

[113] J. K. Bloomfield, E. E. Flanagan, M. Park, and S. Watson, JCAP **1308**, 010 (2013), arXiv:1211.7054 [astro-ph.CO].

[114] L. Amendola, S. Fogli, A. Guarnizo, M. Kunz, and A. Vollmer, Phys. Rev. **D89**, 063538 (2014), arXiv:1311.4765 [astro-ph.CO].

[115] A. Hojjati, JCAP **1301**, 009 (2013), arXiv:1210.3903 [astro-ph.CO].

[116] A. Hojjati, L. Pogosian, A. Silvestri, and G.-B. Zhao, Phys. Rev. **D89**, 083505 (2014), arXiv:1312.5309 [astro-ph.CO].

[117] J. Noller, F. von Braun-Bates, and P. G. Ferreira, Phys. Rev. **D89**, 023521 (2014), arXiv:1310.3266 [astro-ph.CO].

[118] F. Schmidt, Phys. Rev. **D80**, 043001 (2009), arXiv:0905.0858 [astro-ph.CO].

[119] G.-B. Zhao, B. Li, and K. Koyama, Phys. Rev. **D83**, 044007 (2011), arXiv:1011.1257 [astro-ph.CO].

[120] A. Barreira, B. Li, W. A. Hellwing, C. M. Baugh, and S. Pascoli, JCAP **1409**, 031 (2014), arXiv:1408.1084 [astro-ph.CO].

[121] B. Li, A. Barreira, C. M. Baugh, W. A. Hellwing, K. Koyama, S. Pascoli, and G.-B. Zhao, JCAP **1311**, 012 (2013), arXiv:1308.3491 [astro-ph.CO].

[122] P. G. Ferreira and C. Skordis, Phys. Rev. **D81**, 104020 (2010), arXiv:1003.4231 [astro-ph.CO].

[123] G.-B. Zhao, L. Pogosian, A. Silvestri, and J. Zylberberg, Phys. Rev. D **79**, 083513 (2009).

[124] A. Hojjati, L. Pogosian, and G.-B. Zhao, JCAP **1108**, 005 (2011), arXiv:1106.4543 [astro-ph.CO].

[125] F. Feroz, M. P. Hobson, and M. Bridges, Mon. Not. Roy. Astron. Soc. **398**, 1601 (2009), arXiv:0809.3437 [astro-ph].

[126] D. Foreman-Mackey, D. W. Hogg, D. Lang, and J. Goodman, Publ. Astron. Soc. Pac. **125**, 306 (2013), arXiv:1202.3665 [astro-ph.IM].

[127] J. Zuntz, M. Paterno, E. Jennings, D. Rudd, A. Manzotti, S. Dodelson, S. Bridle, S. Sehrish, and J. Kowalkowski, Astron. Comput. **12**, 45 (2015), arXiv:1409.3409 [astro-ph.CO].

[128] J. Schaye, C. Dalla Vecchia, C. M. Booth, R. P. C. Wiersma,

T. Theuns, M. R. Haas, S. Bertone, A. R. Duffy, I. G. Mc-Carthy, and F. van de Voort, Mon. Not. Roy. Astron. Soc. **402**, 1536 (2010), arXiv:0909.5196 [astro-ph.CO].

[129] J. Blazek, N. MacCrann, M. A. Troxel, and X. Fang, ArXiv e-prints (2017), arXiv:1708.09247.

[130] E. Krause *et al.* (DES Collaboration), submitted to Phys. Rev. D (2017), arXiv:1706.09359 [astro-ph.CO].

[131] V. Desjacques, D. Jeong, and F. Schmidt, Phys. Rept. **733**, 1 (2018), arXiv:1611.09787 [astro-ph.CO].

[132] T. Lazeyras, C. Wagner, T. Baldauf, and F. Schmidt, JCAP **1602**, 018 (2016), arXiv:1511.01096 [astro-ph.CO].

[133] G. M. Bernstein, Astrophys. J. **695**, 652 (2009), arXiv:0808.3400 [astro-ph].

[134] R. de Putter and M. Takada, Phys. Rev. **D82**, 103522 (2010), arXiv:1007.4809 [astro-ph.CO].

[135] N. Padmanabhan *et al.*, Mon. Not. Roy. Astron. Soc. **378**, 852 (2007), astro-ph/0605302.

[136] A. Lewis, "GetDist Notes," https://cosmologist.info/notes/GetDist.pdf.

[137] O. S. Center, "Ohio supercomputer center," http://osc.edu/ark:/19495/f5s1ph73 (1987).

[138] N. A. Nystrom, M. J. Levine, R. Z. Roskies, and J. R. Scott (ACM, New York, NY, USA, 2015) pp. 30:1–30:8.

Appendix A: `CosmoSIS` and `CosmoLike` comparison in the context of testing gravity

In the course of our analyses, we have compared the parameter estimation code `CosmoSIS` [127] used in Y1KP to the `CosmoLike` [63] code. The two codes show excellent agreement within the statistical error bars as shown in [130], giving us confidence that our analysis pipeline is robust. In the present paper, we have made substantial modifications (as described below) to the `CosmoSIS` pipeline, which we use as our principal analysis tool, for the case of the parametrized test of gravity. In order to validate the `CosmoSIS` pipeline, we compare its results to those from `CosmoLike`. We first give a brief description of the `CosmoSIS` and `CosmoLike` pipelines as applied to the case of parametrized tests of gravity and then show the results of this comparison.

The `CosmoSIS` pipeline has been used in Y1KP and is further described in [130]. To apply `CosmoSIS` to modified-gravity model analysis, we adopted the publically available code `MGCAMB`, instead of CAMB, for the computation of the matter and CMB power spectra. `MGCAMB` doesn't come with the parameterization of modified gravity identical to ours, so we analytically translate our (Σ_0, μ_0) parameters into `MGCAMB`'s (γ, μ). We use the January 2012 version of `MGCAMB` to perform the systematics checks, and the more recent 2015 version for the constraints on real data. We further modify the part of the pipeline that projects the matter power spectrum into clustering and weak lensing power spectra in order to account for the modified-gravity parameters.

While `MGCAMB` embedded in `CosmoSIS` pipeline modifies the perturbed gravitational potentials and the CMB source functions, `CosmoLike` directly modifies the lensing kernel with Σ_0 and the growth factor with μ_0. The two pipelines should be equivalent except for the ISW effect which is implemented in `MGCAMB` and not in `CosmoLike`. We therefore
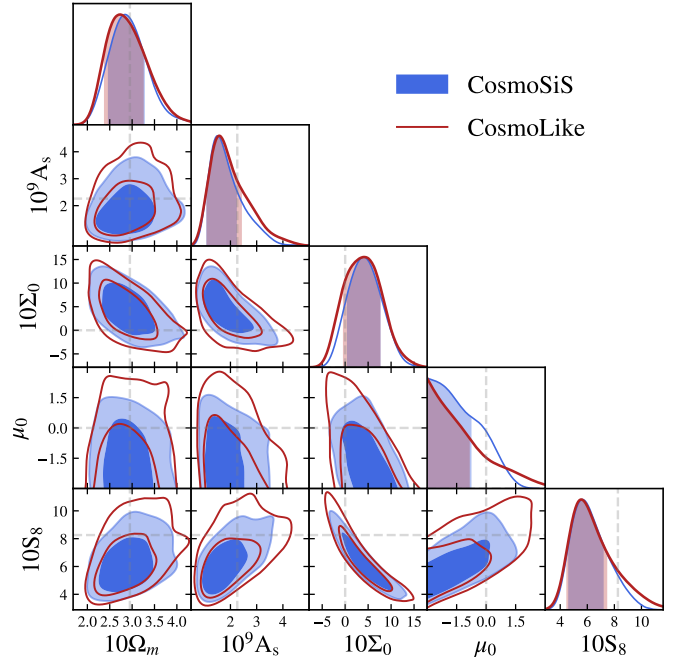

FIG. 8. Constraints on Ω_m, A_s, S_8, Σ_0 and μ_0 using DES Y1 synthetic data for `CosmoSIS` (blue contours) and `CosmoLike` (red).

expect significant differences in the low multipole part of the CMB power spectra, but not elsewhere.

First, we have checked that the weak lensing and clustering observables $\xi_\pm(\theta)$, $\gamma_t(\theta)$, $w(\theta)$ as computed by `CosmoSIS` and `CosmoLike` agree well (difference well below the DES Y1 error bars) for a few sets of (Σ_0, μ_0) values.

Second, we explicitly test the consistency of the `CosmoSIS` and `CosmoLike` pipelines, comparing the constraints they report in the full parameter space. To do this we use the `emcee` sampler on synthetic DES Y1 data, varying the parameters over the prior ranges used in the main analysis. Fig. 8 shows the results for `CosmoSIS` (blue) and `CosmoLike` (red) for a subset of the parameters, namely Ω_m, A_s, σ_8, Σ_0 and μ_0. The two pipelines give similar results, with the 1σ contours agreeing very well for all parameters plotted. However the 2σ contours are wider for `CosmoLike` in some cases, specifically for pairs of parameters including the modified gravity parameter μ_0. This difference is most striking in the (Σ_0, μ_0) plane. This is due to `MGCAMB` failing for sets of (Σ_0, μ_0) in extreme areas. Thanks to its implementation of the modified gravity parameters, `CosmoLike` does not have this issue and is therefore able to explore a wider range of (Σ_0, μ_0). In particular for this case of synthetic DES Y1 data, the 2-σ contours as derived from `CosmoLike` extends to more positive μ_0 than in `CosmoSIS`. This partially explains the constraints on μ_0 from the real DES Y1 data shown in Fig. 4 in the area where μ_0 is very positive. However we note that using the more constraining data sets place us far from these more extreme areas and therefore these results are safe from this issue.